



Three-dimensional CFD modelling of PEM fuel cells

DOI:

[10.1016/j.ces.2009.01.060](https://doi.org/10.1016/j.ces.2009.01.060)

[Link to publication record in Manchester Research Explorer](#)

Citation for published version (APA):

Dawes, J. E., Hanspal, N., Family, O. A., & Turan, A. (2009). Three-dimensional CFD modelling of PEM fuel cells: an investigation into the effects of water flooding. *Chemical Engineering Science*, 64(12), 2781-2794. <https://doi.org/10.1016/j.ces.2009.01.060>

Published in:

Chemical Engineering Science

Citing this paper

Please note that where the full-text provided on Manchester Research Explorer is the Author Accepted Manuscript or Proof version this may differ from the final Published version. If citing, it is advised that you check and use the publisher's definitive version.

General rights

Copyright and moral rights for the publications made accessible in the Research Explorer are retained by the authors and/or other copyright owners and it is a condition of accessing publications that users recognise and abide by the legal requirements associated with these rights.

Takedown policy

If you believe that this document breaches copyright please refer to the University of Manchester's Takedown Procedures [<http://man.ac.uk/04Y6Bo>] or contact uml.scholarlycommunications@manchester.ac.uk providing relevant details, so we can investigate your claim.



Author's Accepted Manuscript

Three-dimensional CFD modelling of PEM fuel cells
An investigation into the effects of water flooding

J.E. Dawes, N.S. Hanspal, O.A. Family, A. Turan

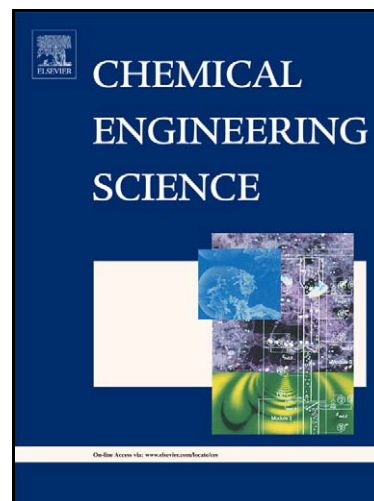
PII: S0009-2509(09)00056-6
DOI: doi:10.1016/j.ces.2009.01.060
Reference: CES 8388

To appear in: *Chemical Engineering Science*

Received date: 28 January 2008
Revised date: 17 January 2009
Accepted date: 20 January 2009

Cite this article as: J.E. Dawes, N.S. Hanspal, O.A. Family and A. Turan, Three-dimensional CFD modelling of PEM fuel cells An investigation into the effects of water flooding, *Chemical Engineering Science* (2009), doi:[10.1016/j.ces.2009.01.060](https://doi.org/10.1016/j.ces.2009.01.060)

This is a PDF file of an unedited manuscript that has been accepted for publication. As a service to our customers we are providing this early version of the manuscript. The manuscript will undergo copyediting, typesetting, and review of the resulting galley proof before it is published in its final citable form. Please note that during the production process errors may be discovered which could affect the content, and all legal disclaimers that apply to the journal pertain.



www.elsevier.com/locate/ces

1 **Three-Dimensional CFD Modelling of PEM Fuel Cells**
2 **An Investigation into the Effects of Water Flooding**

3 **J.E. Dawes¹, N.S. Hanspal², O.A. Family² & A. Turan²**

4
5 *1. Manchester Interdisciplinary Biocentre,*
6 *University of Manchester, M17DN, UK*

7 *2. Energy, Environment and Climate Change Group,*
8 *Energy & Multiphysics Group,*
9 *School of Mechanical, Aerospace and Civil Engineering,*
10 *University of Manchester (UMIST), M601QD, UK*

11
12 **Abstract**

13 In this work, a three-dimensional PEM fuel cell model has been developed and is used to investigate the
14 effects of water flooding on cell performance parameters. The presence of liquid water in the cathode gas diffusion
15 layer (GDL) limits the flow of reactants to the cathode catalyst layer, thereby reducing the overall reaction rate and
16 curtailing the maximum power that can be derived from the cell. To characterize the effects of water flooding on gas
17 diffusion, effective diffusivity models that account for the tortuosity and relative water saturation of the porous fuel
18 cell electrodes have been derived from percolation theory and coupled with the CFD model within a single phase
19 flow skeleton. The governing equations of the overall three-dimensional PEM fuel cell model, which are a
20 representative of the coupled CFD and percolation theory based effective diffusivity models, are then solved using
21 the finite volume method. Parametric studies have been conducted to characterize the effects of gas diffusion layer
22 permeability, inlet humidity and diffusivity of the reactants on the various cell performance parameters such as
23 concentration of reactants/products and cell current densities. It is determined that the gas diffusion layer
24 permeability has little or no effect on the current densities due to the diffusion dominated nature of the gas flow.
25 However, through the incorporation of percolation theory based effective diffusivity model; a marked reduction in
26 the cell performance is observed which closely resembles published experimental observations. This is a reasonable
27 approximation for effects of water flooding which has been inherently used for further parametric studies.

28 **Keywords:** PEM fuel cells, Percolation theory, Electrochemistry, Fluid mechanics, Porous media.

31 1. Introduction

32 Proton exchange membrane (PEM) fuel cells with hydrogen as the fuel are envisioned to be the next
33 generation environmental friendly energy alternatives (Hirschenhofer, 1994; Fontes & Nilsson, 2001) as they have
34 promising applications in the automotive and power sector due to factors such as low operating temperatures with
35 zero/low emissions, a modular structure, quick start-up times, high power density and corrosion resistance (Larminie
36 & Dicks, 2000). Hence, efforts targeted towards gaining an in-depth understanding of the dominant multi-physics
37 within a fuel cell can aid in making them commercially viable and providing the desired power output/energy gains.
38 Computational fuel cell models prove to be a valuable tool for engineers as they help in undertaking reliable
39 simulations, and design optimization studies, facilitate the introduction of cheaper materials/fabrication techniques
40 and provide cost/time effective solutions to appraise the design of complicated cell configurations. However, to date
41 there have been no complete and generic computational PEM fuel cell models (Biyikoglu, 2005) that can account
42 for all the complexities associated with the underlying multi-physics in a single mathematical framework.

43 The performance of a PEM fuel cell depends markedly on the water content (Sousa Jr. *et al.*, 2005) within the
44 polymer membrane. Dehydration of the cell affects the proton resistance of the polymer membrane and electrolyte in
45 the cathode catalyst layer and can reduce performance due to an increase in the voltage across the membrane
46 (Larminie & Dicks, 2000; Yi *et al.*, 2004). To avoid dehydration of the polymer electrolyte, the inlet flows of
47 reactants are often injected mixed with water vapour. However, with excess water production and low diffusion flux
48 (reducing the rate of water-disposal), condensation may occur in the cathode porous layer, clogging the pores and
49 blocking the transport of species to the reaction sites. For these reasons, water management within a PEMFC is a
50 critical issue (Mazumder & Cole, 2003 a&b), especially during prolonged periods of operation.

51 Despite this, the majority of CFD models for PEM fuel cells either do not consider the effects of liquid-water
52 flooding on cell performance or use simplistic assumptions. In the last decade or so there have been various
53 analytical, semi-empirical, one-dimensional and two-dimensional PEMFC models that have been proposed by
54 Bernardi *et al.*(1990, 1992), Springer *et al.*(1991), Fuller & Newman (1993), Nyugen *et al.*(1993), Amphlett *et*
55 *al.*(1995), Standaert *et al.*(1996,1998), Bevers *et al.*(1997), Hubertus *et al.*(1998), Gurau *et al.*(1998), Yi *et*
56 *al.*(1998), Eikerling *et al.*(1998), Wohn *et al.*(1998), Singh *et al.*(1999), Scott *et al.*(2000), Squadrito *et al.*(1999),
57 Baschuk *et al.*(2000), Dannenberg *et al.*(2000), Hsing *et al.*(2000), Um *et al.*(2000), Rowe *et al.* (2001), Maggio *et*

58 *al.*(2001), Wang *et al.*(2001), Eaton *et al.*(2001), Chan *et al.*(2003), Natarajan *et al.*(2003), Maxoulis *et al.*(2004)
59 and Siegel *et al.*(2004).

60 The earliest models by Bernardi *et al.*(1990, 1992), Springer *et al.*(1991) and Nyugen *et al.*(1993) were semi-
61 empirical in nature; based on membrane experimental data used for the calibration of curves. More advanced two-
62 dimensional modelling studies can be attributed to Wang *et al.* (2001). They studied the effects of two-phase flow
63 and transport of reactant gases within the cathode by applying a multiphase mixing model. Single and two-phase
64 transport regimes were discussed and developed analytically (one-dimensionally), allowing simple quantification of
65 the two separate regimes. They simulated the transition between the water phases occurring at a threshold current
66 density value which corresponds to the first appearance of liquid water at the interface between the membrane and
67 the cathode. Despite the model being fairly comprehensive, their studies were limited to cathode zone simulations;
68 as a result it is unclear as to how well the model would cope with full PEMFC simulations.

69 Later, You & Liu (2006) developed a 2-D, two-phase multi-component mixture model to describe the two-
70 phase flow field in the flow channel and the GDL. This model was based on a multi-component mixture model
71 proposed by Wang & Cheng (1997)., The study considered the effects of two-phase flow on convection/diffusion
72 and species transport. Polarization curves under different cathode pressures were simulated and validated against
73 the experimental studies conducted by Huang (2000). They concluded that with an increase of the cathode pressure,
74 both the oxygen molar concentration and exchange current density increase resulting in enhanced fuel cell output
75 voltage for a given over-potential.

76 Analytical, semi-empirical, 1-D and 2-D modeling studies are sufficient for predicting cell performance in
77 the rate limited regimes, however, when mass transport limitations arise they tend to be highly inadequate as the
78 effects of cell geometrical configurations on mass transport are not accounted for. Hence, in the context of design
79 optimization efforts that would make PEM fuel cells commercially feasible, 3-D CFD modeling studies are
80 imperative as they help in gaining better understanding of the realistic physical phenomena associated with the bulk
81 flow in the gas channels and the orthogonal flow within the electrodes and parallel to the membrane.

82 Dutta *et al.* (2000, 2001) developed a 3-D fuel cell model.. The developed models were capable of solving
83 for species concentrations along the gas channels and current density over the membrane surface. This model was
84 configured to match a number of different flow cases from the work of Yi *et al.*(1998) and Fuller *et al.* (1993)
85 investigating dry oxygen and humidified air cases and co-flow/counter-flow cases. The effect of porosity on the

86 diffusion coefficient was accounted for by arbitrarily decreasing the binary diffusion coefficients by 50% rather than
87 using a more comprehensive Bruggeman correlation. Linear extrapolation was used to allow grid independence by
88 interpolating species concentrations on the catalyst layer surfaces. The model was used to investigate two-
89 dimensional current density distributions, which is only possible with a three dimensional model, and the width-
90 averaged current density distributions across the membrane.

91 Mazumder *et al.* (2003a) presented a rigorous 3-D model for PEM fuel cells with no liquid water transport
92 present. Later, (Mazumder *et al.* (2003b)) extended this PEMFC model, predicting water transport effects on cell
93 performance. The resultant model could qualitatively predict the effects of water flooding, however, due to a lack of
94 data for electro-osmotic drag and capillary diffusion coefficients, the numerical predictions still over-predicted the
95 experimental polarization curves at high current densities. The capillary diffusion co-efficient models used
96 correspond to the ones used by Wang *et al.* (2001), however, the numerical values used still remain uncertain. Phase
97 change effects associated with water vapour condensation were tackled by assuming equilibrium phase
98 transformations. This assumption is reasonable as a comprehensive two-phase flow analysis makes the PEMFC
99 model computationally expensive. While the idea was generally sound, the scaling factors they considered in their
100 simulations are still questionable. Key results from their studies indicate that 3-D simulations through inclusion of
101 clogging effects are imperative to accurately capture the localised water saturation levels and cell voltage-current
102 characteristics in comparison to 2-D modelling.

103 Um & Wang (2004) presented a 3-D CFD model including gas channels and MEA similar to that of Dutta *et*
104 *al.* (2000, 2001). A single domain model features a detailed MEA water transport model which was used to compare
105 two different flow-fields, namely straight and inter-digitated patterns. Their model shows that forced convection
106 created by the use of inter-digitated flow-fields, (through the use of a positive pressure gradient) improves the flow
107 of oxygen to the cathode catalyst layer and improves the removal of water enhancing the overall performance of the
108 cell.

109 Nguyen *et al.* (2004) modelled a PEMFC under a single-phase flow assumption, and considered a serpentine
110 flow field (modelling a repetitive unit of the serpentine channel). Diffusion in the porous zones was computed using
111 the Stefan-Maxwell equation and the Bruggeman correlation. The membrane was considered to be fully humidified.
112 A unique feature of the model was to use an electrical voltage-to-current algorithm that computes the local over
113 potential by solving for the potential field. The results are significantly different from cases where a constant surface

114 over potential is assumed. As with all single-phase models there was significant discrepancy found between the
115 model and experimental results at high current densities due to the effects of water flooding.

116 Lum *et al.* (2005) presented a steady-state, three dimensional, isothermal model of a full PEM fuel cell,
117 similar to that of Dutta *et al.*(2000),. The model was single-phase, only considering the vapour phase of water. This
118 model was validated both globally and locally at points along the gas channel using experimental data from a
119 segmented fuel cell.. A deviation from experimental results was found at high current density/high humidity due to
120 liquid water flooding. However, at a lower humidity/current density, excellent agreement with the experimental data
121 was observed. It was found that there was a limiting permeability below which very little performance deterioration
122 will occur as in the gas diffusion layers the flow is diffusion dominated, which has also been observed in this study.
123 This is not observed experimentally. In practice permeability will have a marked effect as liquid water will directly
124 affect the reactant flow rates and result in a significant performance drop, especially in fuel cells facilitated by
125 forced convection such as inter-digitated flow-fields.

126 Sivertsen & Dijali (2005) developed a 3-D single phase, non-isothermal PEMFC computer model, accounting
127 for distributed overpotential at the cathode catalyst layer and heat sources at each electrode, also incorporating, heat
128 transfer in the solids and gases. Mass transport was described by the Stefan-Maxwell equations by calculating binary
129 diffusion coefficients. To account for additional drag caused by the irregular shape and length pore scales, an
130 effective diffusion coefficient was used in the simulations, which assumes a constant tortuosity factor of 3. The
131 water transport phenomenon was based on the model proposed by Janssen (2001) The studies show that changing
132 the conductivity radically alters the current density.

133 Jiao *et al.* (2006) simulated 3-D straight micro-parallel-channels with inlet and outlet manifolds for a PEM
134 fuel cell stack using a volume of fluid (VOF), two-phase flow model under different initial water concentrations.
135 The effects of surface tension and wall-adhesion were modelled using the continuum surface force (CSF) model
136 proposed by Brackbill *et al.* (1992). Their parametric studies resulted in numerous design recommendations related
137 to alleviating the water flooding problem, such as, proposition of serpentine gas-flow channels, inlet/outlet
138 manifolds with reduced/increased cross-sectional area respectively, curved wall facing the air flow inlet and
139 selection of materials with less water adhesion effects.

140 Although most of the recent 3-D modelling studies are fairly comprehensive, the majority directly concern
141 issues related to either flow-optimization, natural convection on the cathode side, or to the comparison of straight

142 and inter-digitated flow-fields, ignoring the effects arising from multi-physics and coupled flow/mass-transport in
143 the process. The remainder of the 3-D PEMFC studies that considering water-flooding are either based on simplistic
144 treatments such as arbitrarily altering the conductivity/binary diffusivities, neglecting changes in
145 porosity/permeability, assuming no interaction between phases in sub-domains or including artificial parameters in
146 water transport models which cannot be determined experimentally. The attempt of this work is to focus on such
147 simplistic assumptions and re-consider the use of diffusivity models derived from the percolation theory, that are
148 computationally inexpensive, to investigate the effects of water flooding.

149 Selyacov *et al.* (1996) gave an overview of the application of percolation theory to the modelling of transport
150 in porous media. Analytical methods for determining conductivity parameters, such as electrical conductivity and
151 permeability were presented. These methods are derived using microscopic flow models and percolation
152 relationships, considering single and multiphase flows. Pharoah *et al.* (2006) later reviewed the approaches adopted
153 to model the effective transport coefficients, chemical species diffusivity, electrical conductivity, thermal
154 conductivity and the hydraulic permeability of carbon-fibre based porous electrodes in PEM fuel cells.

155 Nam & Kaviany (2003) were the first to study in detail the effects of the formation/distribution of condensed
156 water in PEM fuel cell diffusion medium on cell performance by a reduction in effective mass diffusivity. A local
157 mass-diffusivity model of a fibrous diffusion medium was developed as a function of the local porosity and water
158 saturation, using a computational network-model, considering the structure of the GDL as stacks of randomly shifted
159 grids with constant pore size, for species diffusion.. Diffusion was then solved over a cubic grid considering face
160 and edge diffusion between connected cells.. Close agreements were obtained against the results of Tomadakis *et al.*
161 (1993). The mass diffusivity model was then used in conjunction with the capillary hydrodynamics, two-phase flow
162 behaviour, water formation rate and the condensation kinetics to determine the 1-D distribution of water saturation.
163 Tseng *et al.* (2005) performed numerous experiments to study the structure effects of gas diffusion layer (GDL) and
164 microporous layer (MPL) characteristics on the water management/performance of a PEM fuel cell. The pore-size
165 range, pore-size distribution, pore-structure, surface contact angle, electric contact resistance and internal structure
166 (i.e. pore-size distribution and gas-permeability) were determined, using scanning electron microscopy (SEM),
167 porosimetry, and a surface contact angle meter, to investigate their effects on cell performance.. Finally they
168 investigated the effects of MPL, thickness of MPL, PTFE loadings and the type of carbon black used in MPL on the
169 cell performance.

170 In the current study, the effects of liquid water-flooding are investigated by considering a single-phase 3-D
171 PEM fuel cell model, (similar to models developed by Springer *et al.* (1991), Dutta *et al.* (2000) and Lum *et al.*
172 (2005) amongst others) in conjunction with effective diffusivity models derived from percolation theory based on
173 the works of Selyacov *et al.* (1996), Nam *et al.* (2000) and Tseng *et al.* (2005). This work's parametric studies focus
174 on simulating design parameters of interest such as average current density and its dependence on water-flooding
175 which are related to the effective diffusivity variations. The investigations are based on a repeating section of gas
176 channels, gas diffusion layers, catalyst layers and membrane.

177 The single phase assumption proves to be a computationally economic alternative in comparison to the costly
178 two-phase flow simulations. The liquid water saturations for use in the water-flooding model are predicted using the
179 relative-humidity values and water-vapour volume fractions, instead of the method suggested by Um and Wang
180 (2004). Results from our model have been validated against the experimental and computational data of Shimpalee
181 *et al.*(1999) and Lum *et al.*(2005).

182 **2. Mathematical statement of the problem**

183 The 3-D numerical model consists of two gas channels transporting hydrogen and oxygen reactants and water
184 vapour (the product) mixed in air (nitrogen) to and from two porous gas diffusion layers (GDLs). The GDLs in turn
185 transport the gases to and from the catalyst layers where all the electrochemical reactions occur. The catalyst layers
186 sandwich a membrane through which protons and water are transported. The governing equations for the gas
187 channels, GDLs and catalyst layers consist of continuity, conservation of momentum and species transport. Source
188 terms are applied at the catalyst layers to represent the electrochemistry and transport through the membrane. In
189 order to model these source terms the local current density (used to determine reaction rates) and net water transport
190 coefficient (used to determine transport across the membrane) are calculated using auxiliary models which have
191 been linked to the main flow solver through UDFs (User Defined Functions).

192 The liquid phase of water is not directly modelled. This simplification significantly reduces the complexity of
193 the simulation; removing the need to model phase changes and allowing for an isothermal steady state simulation
194 which is a valid assumption for low-temperature PEMFC applications.

195 **2.1 Governing Equations**

196 The Navier-Stokes equations, consisting of the momentum equations (eqn. 1), the continuity equation (eqn.
197 3) and species transport (eqn. 6) were used to model the flow of the four modelled species (under the assumption of

198 laminar flow and steady state) in the in the gas channels, GDLs and catalyst layers. The porous nature of the GDLs
 199 and catalyst layers was accounted for by the addition of a Darcy's law term to the momentum equations to represent
 200 the momentum associated with the surface forces in these porous zones. In this study the porous structures are
 201 assumed to be isotropic.

202 Fick's Law of diffusion (Bird *et al.*, 1960) was used to account for multi-component mass transport in the gas
 203 diffusion layers. In anode only two species namely hydrogen and water vapour are present whereas in cathode
 204 oxygen, nitrogen and water vapour are dominant. Although Fick's law ignores the species-species interactions, in
 205 this study we have considered each species diffusing within an approximate carrier fluid which tends to reduce this
 206 limitation. This assumption is further proven to be reasonable, as can be seen from figure 3, where the current
 207 densities predicted by Lum *et al.* (2004) who used Stephan-Maxwell multi-component diffusion, and our model are
 208 nearly identical. In addition, the species transported within the fuel cell are relatively dilute (Gallart, 2007), which
 209 further justifies the use of Fick's Law in this particular study. This in effect leads to a slight overestimation of
 210 species diffusivity. The binary (oxygen, hydrogen or water vapour in air) diffusivity coefficients are calculated
 211 using the mass fractions, pressure, temperature, critical temperature and the critical pressures of the two components
 212 (eqn. 11) based upon the works of Slattery *et al.* (1958). The governing equations and source terms are shown below
 213 in table 1.

Table 1

214
 215 The catalyst layer reactions and species transport across the membrane were added to the Navier Stokes
 216 equations as volumetric source terms to the continuity equation (S_m) and species transport equations (S_k). These
 217 source terms are defined as zero in all regions except the catalyst layers and represent the consumption of hydrogen
 218 at the anode (S_{H_2}), the consumption of oxygen at the cathode (S_{O_2}), the production and flux (due to electro-osmotic
 219 drag and back diffusion) of water at the cathode (S_{cw}) and the flux of water (due to electro-osmotic drag and back
 220 diffusion) at the anode (S_{aw}). In the continuity equations the source terms for all species are summed, whereas in the
 221 species continuity equation each is applied to its own species transport equation.
 222 The source terms in relation to the current density $I(x,y)$ and the net water transport coefficient $\alpha(x,y)$ are shown in
 223 table 2. The current density and net water transport coefficient are determined using the auxiliary equations
 224 discussed in the subsequent section.

Table 2

225

226 **2.2 Auxiliary model equations**

227 The auxiliary equations model the electrochemical reactions and determine the net water transport
228 coefficient and local current density, and in turn volumetric source terms. These equations are provided in table 2.
229 The empirical equations used in this work are based on Nafion 117, and can be referred to in works by Springer et
230 al. (1993). A concise description of the auxiliary models is given below, a more detailed account can be found in
231 Lum *et al.* (2005) and Dutta *et al.* (2000)) amongst others.

232 The net water transport coefficient (eqn. 12) is used to determine the transport of water vapour across the
233 membrane and relates the relative magnitudes of back-diffusion from the cathode to the anode and the electro-
234 osmotic drag. It is determined using the electro-osmotic drag coefficient (eqn. 20) and the water diffusion coefficient
235 (eqn. 21). The electro-osmotic drag coefficient (eqn. 20) is an empirical relationship based on the water activity
236 (eqn. 18) which is in turn affected by the saturation vapour pressure (eqn. 19) which is modelled empirically and
237 referred in the work of Weast et al. (1981). The water diffusion coefficient depends on the electro-osmotic drag
238 coefficient, the temperature, water concentration (eqns. 16-7) at the anode and cathode (which depend on the water
239 activity), the dry mass and density of the membrane and the local current density.

240 The local current density (eqn. 13) defines the proton flux across the membrane, and hence the proton flux
241 associated with each reaction which in turn defines the reaction rate. The local current density depends on the
242 membrane conductivity, which is modelled using an empirical relationship (eqn. 15) which relates it to the
243 membrane dry mass, dry density and water concentration and assumes no swelling of the membrane. The local
244 current density also depends on the membrane thickness, open circuit and cell voltages and the reaction
245 overpotential. The reaction overpotential is modelled using the Tafel equation (eqn. 14) (Tafel *et al.*, 1905) which in
246 turn depends on the partial pressure of oxygen, the temperature, the cell voltages, the exchange current density and
247 the local current density. Due to this implicit relationship between the current density and overpotential, these two
248 equations are solved iteratively using the Secant method (which is employed because of its stable nature). This work
249 neglects the contribution of the anode reaction to the cell overpotential as the exchange current density is an order of
250 magnitude smaller.

251 The empirical relations and data fits used in this study have proved sufficient for many previous studies (Lum
252 *et al.* (2005), Dutta *et al.* (2000)), and so are deemed sufficient in this work.

253 The diffusivity of each species is altered using a percolation-type diffusivity model. It is further assumed that each
 254 species is present in a carrier fluid i.e. air in this case and hence the equation is used to calculate the diffusivity of
 255 each species in air.

256 **2.3 Effective Diffusivity model**

257 The effective diffusivity model accounts for the effects of water-saturation and porosity by multiplying the
 258 Fickian diffusion coefficients for each species by scaling functions of water saturation and porosity (eqn. 22) before
 259 use the species transport equations (eqns. 6). Mathematically this can be written as

$$260 \quad D_{eff} = D f(\varepsilon)g(S) \quad [22]$$

261 The gas diffusion layer (GDL) is typically made out of carbon-cloth in the form of a high porosity
 262 overlapping fibre structure. The effective diffusivity in such a medium can be related to the electrical conductivity
 263 by the Nernst-Einstein equation (Garboczi *et al.* (1992)).

264 The GDL electrical conductivity obeys simple scaling laws. Therefore the correlation length and the number
 265 of parallel conducting bonds per unit cross-sectional area in the GDL can be determined as a function of the bond
 266 occupation probability P_b and the percolation threshold P_{bc} using the following equations

$$267 \quad \xi \propto (P_b - P_{bc})^{-\nu} \quad [23]$$

$$268 \quad n = \frac{1}{\xi^2} \quad [24]$$

269 Where ξ is the correlation length, n is the number of parallel conducting bonds per unit cross sectional area, ν
 270 is the critical exponent and P_b and P_{bc} are the bond occupation probability and percolation threshold respectively.

271 As the conductivity is proportional to the number of parallel conducting bonds per unit cross-sectional area,
 272 by using equations 23 and 24 the scaling laws for the effective diffusivity can be determined, using equation 25

$$273 \quad \frac{\lambda_1}{\lambda_0} = \frac{D_1}{D_0} = \frac{(P - P_{bc})^{2\nu}}{(1 - P_{bc})^{2\nu}} \quad [25]$$

274 Where ν is the correlation index, depending on the dimension of the problem only, λ_1 and λ_0 are
 275 conductivities and D_1 and D_0 are diffusivities corresponding to the current state and the percolation threshold. This
 276 equation (25) compares very favourably to the work of Tomadakis *et al.* (1993).

277 The value of the correlation index and percolation threshold used for the 3-D problem in this work is listed in
 278 Table 3. The bond occupation probability is the conducting fraction of the medium to the phase under consideration;
 279 in the case of the reactant gases this fraction is proportional to the porosity and inversely proportional to the
 280 saturation.

$$281 \quad f(\varepsilon) = \frac{(\varepsilon - P_{bc})^{2\nu}}{(1 - P_{bc})^{2\nu}}, \quad g(S) = \frac{((1 - S) - P_{bc})^{2\nu}}{(1 - P_{bc})^{2\nu}} \quad [26]$$

282 In order to model the effective diffusivity, the saturation within each cell volume must be calculated. The
 283 relative humidity is defined by equation 27.

$$284 \quad \text{Relative humidity} = \frac{P_{H_2O}}{P_w^{sat}} \quad [27]$$

285 Where P_{H_2O} is the partial pressure of water vapour, and P_w^{sat} is the vapour saturation pressure.
 286 In this work it is assumed that if the relative humidity in a control volume is higher than 100% the saturation is
 287 defined as the ratio of the volume of water vapour within each computational cell to the total volume of each
 288 computational cell, otherwise the saturation is zero.

$$289 \quad \begin{aligned} \text{Saturation} &= \frac{\text{vol}_{H_2O}}{\text{vol}_{total}}, \text{ if relative humidity} \geq 100\% \\ \text{Saturation} &= 0, \quad \text{if relative humidity} < 100\% \end{aligned} \quad [28]$$

290 Common approximations to the effects of saturation and diffusivity are also considered (namely the
 291 Bruggeman coefficient (eqn. 29) and a power law (eqn. 30)) and compared to the use of the analytical model from
 292 percolation theory. Both diffusivity models are in the same form as equation 30.

$$293 \quad f(\varepsilon) = \varepsilon^{1.5} \quad [29]$$

$$294 \quad g(S) = (1 - S)^2 \quad [30]$$

295 Model 2 is derived using percolation theory and the Nernst-Einstein equation described previously. This
 296 model can be mathematically represented as equations 2.33 and 2.34.

$$297 \quad f(\varepsilon) = \frac{(\varepsilon - 0.11)^{0.9}}{(1 - 0.11)^{0.9}} \quad [33]$$

$$g(S) = \frac{((1-S)-0.11)^{0.9}}{(1-0.11)^{0.9}} \quad [34]$$

Further details of the flooding models can be found in Dawes (2007) and Dawes *et al.* (2008).

3. Computational Results and Discussions

The governing equations were solved alongside the auxiliary equations using a finite-volume method based on a SIMPLE algorithm (Ferziger *et al.* (2002)). The source terms to model the reactions, the percolation based diffusivity model and the electrochemistry algorithm were written into ANSI C++ User-Defined-Functions (UDFs) which were then interpreted by the main CFD flow-solver FLUENT. A segregated solver was then employed to solve the final coupled set of equations.

A diagram of the solution procedure, showing an overview of the main algorithm and the points at which the sub-algorithms are incorporated is shown in figure 1.

Figure 1

In order to simplify the validation process, the geometry used in this study is identical to that studied by Dutta *et al.* (2000). The geometry represents the thin central portion of a fuel cell, one single channel wide. The computational domain does not extend through the membrane, where water and proton transport is handled using the auxiliary equations.

3.1 Computational model

The source terms are applied to the catalyst layers. These volumetric source terms model the destruction of hydrogen and oxygen, the transport of protons and the transport and creation of liquid water.

At the inlets of the computational domain Dirichlet velocity boundary conditions are applied. At the electrodes outlets, zero velocity gradient ($\nabla u = 0$) and zero species gradient ($\nabla X_k = 0$) boundary conditions are applied. These boundary conditions make the assumption that the flow is fully developed in the gas channels. This assumption is valid since the length of the gas channels is large in comparison to the width of the porous electrodes combined with the membrane. As this model represents a central strip of a much wider fuel cell, a symmetry boundary condition is applied on the top and bottom surfaces of the porous region. A no-slip condition (Ferziger (2002)) is applied to the external walls.

Table 3a

Table 3b

324
325 Table 3a and b list the prescribed boundary condition values (velocities and species concentrations) used for
326 each humidity condition, and the physical parameters respectively.

327 Grid and scheme independence checks were undertaken; it was found that the solution was grid independent
328 for the mesh shown in Figure 4, which contains a total of 14114 hexahedral cells. A scheme independence test found
329 close correlation between the second order upwinding and QUICK schemes, but a large discrepancy with first order
330 upwinding due to the additional artificial diffusion. For this reason second order upwinding was adopted as it proved
331 as accurate as the higher order scheme and reduced computational expense.

332 Figure 2 schematically shows the dimensions of the geometry, the applied boundary conditions and the
333 numerical grid used in this study. Due to the high aspect ratio of this geometry, in all figures the dimensions in the x
334 and y directions are shown scaled up relative to dimensions in the z direction for clarity.

Figure 2

335
336 The physical parameters and boundary conditions used for all simulations are shown in Tables 3 a and b. The
337 humidity conditions considered are the same as those used by Lum *et al.* (2004).

Table 4

338
339 The relevant numerical parameters for this study are shown in Table 4.

340 Results are presented for the developed PEM fuel cell model. Validation is first undertaken by considering
341 constant diffusivity coefficients, in this case the model is numerically similar to current single phase models, such as
342 Lum *et al.* (2004) and Dutta *et al.* (2000) and so easily validated. Results from parametric studies into the effect of
343 diffusivity coefficients and permeability are then presented to justify the development in integration of an effective
344 diffusivity mode. Finally the two effective diffusivity models are incorporated and compared to experimental data.

345 **3.2 Model validation**

346 Figure 3 shows the width averaged current density at the cathode catalyst layer along the channel length for
347 the constant diffusivity very high humidity case. Close agreement is found with the results of Shimpalee *et al.*
348 (2000) who validated their model both globally and locally against experimental data at low and medium current
349 density values; before the transport limitations caused by flooding become significant.

Figure 3

350

351 Good agreement is also found for the other humidity conditions (as can be seen in the global validation in
352 Figure 12). The slight discrepancies between the two models are likely to be due the use of Fick's law rather than
353 the Stefan Maxwell equations, however the close agreement shows that Fick's law is still a reasonable
354 approximation.

355 **3.3 Velocity vectors and pressure distribution**

356 The calculated flow patterns, shown below in Figure 4, show a strong longitudinal flow in the gas channels,
357 and a much slower and proportionally more lateral flow in the porous zones. As the mixture velocity magnitude is
358 significantly larger in the gas channels than in the porous zones, the much slower flow in the porous zones is shown
359 separately (Figure 5) for clarity.

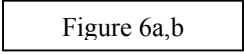
360  Figure 4

361 Comparing the velocity vectors at the first two longitudinally spaced slices shows that despite the inlet being
362 modelled as uniform velocity, the flow takes on its parabolic profile (due to the wall no slip conditions) becoming
363 fully developed on both the anode and cathode side, and the lateral velocities quickly reduce. These developed
364 velocity profiles on both the anode and cathode are shown enlarged. It is important to note that the gas channel-gas
365 diffusion layer interface does not force a no-slip condition as this interface is porous but instead significantly
366 reduces the rate of transport. The flow is significantly faster on the cathode side to match the stoichiometric balance
367 of the reactants required for the reaction on the catalyst layers.

368 The primary flow is pressure driven, with velocity boundary conditions applied at the inlets and lower
369 pressure boundary conditions applied at the outlets, and as such the pressure of the mixture drops nearly linearly
370 from inlet to outlet where the gauge pressure reduces to zero along the anode and cathode gas channels.

371  Figure 5

372 In the porous zones (Figure 5) the velocity magnitude is much slower and is close to lateral in direction,
373 showing a net convection of reactants to the catalyst layer. The flow (especially on the anode side) is defined mostly
374 by the reaction rather than by the large inlet velocities. Transport limitations are of critical importance as they reduce
375 the transport across the porous zones, limit the reaction rates and thus the define current density and power output.

376  Figure 6a,b

377 The pressure distribution within the PEM fuel cell is shown in Figure 6. The lateral slice shows that the
 378 pressure decreases linearly by approximately 970 Pa on the cathode side and 140 Pa on the anode side. The porous
 379 zones cause local variations in pressure, with pressure increasing or decreasing across the porous zones depending
 380 on the relative mixture velocity. These variations are too small (in the order of 1 Pa) in comparison to the
 381 longitudinal pressure drop and the pressure difference between the anode and cathode to be visible globally. A
 382 blown up lateral slice (at $z=0.05\text{m}$) is shown in order to better visualise this small pressure drop. The contours are
 383 curved, different from the usual linear drop expected in simple filtration systems due to the mixture velocity
 384 direction being inwards towards the catalyst layers.

385 *3.3.1 Effect of GDL permeability*

386 Figure 7a,b,c

387 Figure 8a,b,c

388 Figure 7 a, b and c show velocity vectors for three different GDL permeability values ($5 \times 10^{-10} \text{m}^2$, $5 \times 10^{-11} \text{m}^2$
 389 $5 \times 10^{-12} \text{m}^2$). The figures 8a, b and c represent pressure variations at the cathode and anode GDLs at different
 390 longitudinal slices at the inlet, the centre, and the outlet. The arrow direction gives the flow direction and the arrow
 391 colour gives velocity magnitude

392 The flow directions are dependent on the GDL permeability. For high permeability GDL material there is a
 393 much larger longitudinal convection of mixture, with the high speed gas channel flow and large pressure drop
 394 strongly affecting the GDL flowfield. This results in a more complicated flow pattern as can be seen by anode
 395 pressure profile at the outlet. The peak at on the cathode outlet at $x = 0.00187\text{m}$ for the high permeability case
 396 (Figure 8a) reflects the fact that the direction of flow changes, as can be seen in Figure 7a. This change in flow
 397 direction is due to the combination of the flow out of the GDL back into the gas channel and out of the outlets
 398 (because the flow is convecting downstream), and the flow diffusing to the catalyst layers where it is destroyed,
 399 these transport mechanisms effectively act in opposite directions at the wall and, as they are comparable in
 400 magnitude for the high permeability case, they produce the curved peaked profile.

401 Arrow length is kept constant as the velocity magnitudes vary significantly between zones

402 For the lower permeability cases the pressure profiles at the inlet and outlet become more linear. This is
 403 because the flow becomes diffusion dominated so longitudinal convection significantly reduces, shown by the
 404 direction of the velocity vectors at the anode and cathode being close to perpendicular to the gas channels.

405 3.4 Species concentrations

406 Flooding occurs on the cathode catalyst layers, so this is where transport limitations are more relevant, for
407 this reason the species distributions at the cathode are studied.

408 Figure 9

409 Figure 9 shows the distribution of water in both liquid and vapour as assumed in the variable diffusivity
410 models. Contours of water vapour volume fraction are shown at slices along the longitudinal direction. The water
411 vapour volume fraction increases downstream due to pressure gradient driving the longitudinal convection, and due
412 to the depletion of oxygen from the mixture. The water vapour also diffuses inwards towards the gas channels; this
413 effect is caused by the shoulders and results in the curved lateral contours.

414 The iso-surface shows the dew point front, the position where the relative humidity exceeds 100%. Both
415 variable diffusivity models assume that the water vapour condenses to form droplets of liquid water in any cell with
416 a relative humidity above this value, so liquid water is modelled as present above the relative humidity iso-surface.
417 This plot shows that the liquid water it is mostly contained in cathode gas diffusion layer. Physically in this area the
418 water vapour condenses to form droplets of liquid water which block pores in the gas diffusion layer impeding the
419 transport of reactants and hence curtailing the cell performance. So the water vapour volume fraction in these
420 regions simply represents the liquid water saturation. A more detailed phase change and liquid water transport model
421 would clearly improve the model in this region, this however is more suited to a multiphase model and hence
422 beyond the scope of this paper.

423 Figure 10

424 Figure 10 shows the distribution of oxygen in the cathode. Oxygen diffuses from the cathode gas channel
425 through the gas diffusion layer to the catalyst layer where it is destroyed and liquid water created. The oxygen
426 diffuses outwards into the gas diffusion layer and into the shoulders; shown by the curved contours. The oxygen
427 concentration decreases downstream as oxygen is removed from the gas channel and due to the increased volume
428 fraction of water vapour.

429 3.5 Parametric studies

430 In order to model liquid water flooding, the liquid water saturation is related to a limitation in transport. The
431 reactants travel through the cell via convection and diffusion; these modes of transport are limited by diffusivity and
432 permeability. The transport of gases in the porous zones is clearly diffusion dominated and so it was decided to

433 employ a diffusivity model. To check this assumption a study was undertaken to determine the relative importance
434 of phase permeability and reactant diffusivity. The parameters used in these parametric studies are given below in
435 Table 5.

436

Table 5

437

Figure 11

438 A wide logarithmic range of gas diffusion layer permeability values were applied to the model and the
439 resulting width averaged current density plots are shown in Figure 11. From Figure 11 it is clear that any
440 permeability value below $5 \times 10^{-11} \text{m}^2$ (a typical gas diffusion layer permeability and the value chosen for this study)
441 any changes in the current density cease. As the effects of saturation are only going to reduce the reactant phase
442 permeabilities further than the absolute permeability, this parametric study shows that the incorporation of a relative
443 permeability model into the single phase model will not have any effect.

444

Figure 12

445 The simulation was undertaken with a variety of different diffusivity coefficients (see Figure 12). Diffusivity
446 coefficients were scaled up and down (the resulting current density plotted as shown in Figure 14). In this case
447 '100% diffusivity' refers to the diffusivity calculated by equation 24. Each diffusivity coefficient was then increased
448 by 20% and 40% then decreased by 20%, 40% and 60%.

449 With decreasing diffusivity, the local current density and total averaged current density both decrease. The
450 reduction in diffusivity is felt strongly at the inlet of the PEM fuel cell, where the current density is large and the
451 reaction rate and so rate of diffusion from the gas channel to the catalyst layers is very high.

452 Unlike for the permeability parametric study there is a marked decrease in cell performance for realistic
453 changes in diffusivity, so it was decided that the initial assumptions were correct and that a diffusion model alone is
454 sufficient to model flooding in a single phase model.

455

456 *3.6 Local and global validation of flooding PEMFC model*

457

Figure 13

458 As shown in Figure 13 both diffusivity models show a decrease in all local width averaged current density
459 values due to the improved model for diffusion within the porous and saturated zones. The second diffusivity model
460 showed a more marked reduction further downstream.

461 The implementation of second model resulted in a larger decrease in current density, and so produced results
462 closer to the experimental data of Shimpalee *et al.* (1999,2000). Also, as the first widely used model makes the
463 assumption of a face centred cubic bonding structure for the Bruggeman correlation and uses simple approximations
464 for the saturation dependence, whereas the second diffusivity model has been derived by applying percolation theory
465 concepts specifically to the gas diffusion layer material under consideration, and so provides a model more specific
466 to the GDL material.

467 Figure 14

468 The result shown in Figure 14 show that that the use of the analytical diffusivity model results in similar
469 predictions to experiment and to the work of Lum *et al.* (2004) at low and high humidity conditions (humidity
470 conditions referred to are in table 3a.).

471 At very high humidity conditions, the single phase PEM fuel cell model with the second analytical diffusivity
472 model (Model 2) presented in this paper results in a performance drop when water flooding occurs at the cathode
473 catalyst layer. This is an effect not seen in current single phase models, and is more representative of the results
474 found by experiment at high power densities and high humidity conditions.

475 **4. Conclusions**

476 This paper presents the results from a three-dimensional, single-phase, fuel cell model, coupled with an
477 effective diffusivity algorithm derived from the percolation theory for simulating water flooding within PEM fuel
478 cells. The objective of this study was to improve upon the existing single-phase models by making allowances for
479 the drop off in performance associated with liquid water flooding. Conventional single phase models cannot predict
480 this phenomenon, and are thus restricted to low current density and low humidity conditions. The numerical model
481 and its implementation were validated by comparison to the work of Shimpalee *et al.* (1999) using an identical
482 computational grid.

483 Parametric studies were undertaken, consisted of investigations into the effects of diffusivity and
484 permeability, to determine the best way to model the transport restrictions caused by liquid water flooding.
485 Lowering diffusivity coefficients resulted in a reduction in the cell current densities. Lowering the GDL

486 permeability only affected the local current density up to limiting permeability value; a value greater than the
487 realistic, unsaturated gas diffusion layer permeability value used. A phase permeability model could only reduce the
488 permeability further than this initial value, so the incorporation of a phase permeability model would not affect the
489 cell current density or any other performance parameters. Hence it was concluded that an accurate diffusivity model
490 would increase the accuracy of the results, whereas for a single phase model at least, a phase permeability model
491 would leave the cell performance unaffected. This however is not shown and a phase permeability model specific to
492 the gas diffusion layer material has been developed for use in multiphase simulation.

493 Simulations were carried out for three sets of physical parameters representing three different humidity cases
494 to study the accuracy of the model for a wide range of conditions, as has also been done by Lum *et al.* (2004) and
495 Dutta *et al.* (2000). The incorporation of the effective diffusivity model resulted in the prediction of cell current
496 densities which were closer to those predicted experimentally at higher current densities without the loss of accuracy
497 at lower current densities.

498 There is still however much room for improvement, as the developed model does not consider the transport of
499 liquid water, which for greater accuracy should certainly be modelled separately. Although the diffusivity model
500 improves the predictive power of the numerical model, a multiphase model would represent a significant
501 improvement and allow for the correct treatment of diffusion and convection of the reactant gases and liquid water.
502 This liquid water will not be diffusion dominated within the gas diffusion layer. Hence a significant benefit could be
503 achieved by employing the developed effective diffusivity models (Model 2) resulting from this work, in
504 conjunction with a model capable of simulating phase-permeabilities in a multiphase solution.

505

505 **Nomenclature**

506	a_k	- Water activity	542	ϵ	- Porosity
507	a	- Pressure diffusivity constant	543	ξ	- Correlation length
508	b	- Pressure diffusivity constant	544	λ	- Electrical conductivity
509	c	- Concentration	545	μ	- Dynamic viscosity
510	D_k	- Diffusivity coefficient	546	ρ	- Density
511	$D_{k,j}$	- Binary diffusion coefficient	547	$\sigma_{m(x,y)}$	- Membrane conductivity
512	D_k^{eff}	- Effective diffusivity of species	548	ν	- Critical exponent
513	DSF	- Diffusivity scaling factor	549	Subscripts	
514	F	- Faraday's constant	550	A	- First component
515	$f()$	- Diffusivity scaling function	551	a	- anode
516	$g()$	- Diffusivity scaling function	552	B	- Second component
517	$I(x,y)$	- Current density	553	c	- Cathode
518	I_0	- Exchange current density	554	Dry	- Dry membrane
519	J	- Binary diffusion coefficient	555	H_2	- Hydrogen
520	k	- Permeability	556	i	- Direction
521	M	- Molar mass of species	557	k	- Species
522	$M_{m,dry}$	- Mass of dry membrane	558	m	- Membrane
523	n	- Number of bonds	559	O_2	- Oxygen
524	$n_d(x,y)$	- Electro-osmotic drag coefficient	560	w	- Water
525	P	- Pressure	561	x	- x direction
526	P_b	- Bond occupation probability	562	y	- y direction
527	P_w^{sat}	- Saturation pressure of water	563	z	- z direction
528	R	- Universal gas constant	564	0	- Unsaturated
529	S	- Saturation	565	1	- Partially saturated
530	S_u	- Momentum source	566	Superscripts	
531	S_k	- Species transport source	567	sat	- Saturation
532	T	- Temperature	568	eff	- Effective
533	t_m	- Membrane thickness			
534	u	- Velocity			
535	V_{oc}	- Open circuit voltage			
536	V_{cell}	- Cell voltage			
537	V_{ol}	- Volume fraction			
538	X	- Molar mass fraction			
539	Y	- Mole fraction			
540	$\alpha(x,y)$	- Net water transport coefficient			
541	$\eta(x,y)$	- Local overpotential			

References

- Amphlett, J. C., E. H. de Oliveira, et al. (1997). "Dynamic interaction of a proton exchange membrane fuel cell and a lead-acid battery." *Journal of Power Sources* **65**(1-2): 173-178.
- Baschuk, J. J. and X. Li (2000). "Modelling of polymer electrolyte membrane fuel cells with variable degrees of water flooding" *Journal of Power Sources* **86**(1-2): 181-196
- Brackbill J. U., D. B. Kothe, C. Zemach (1992). "A continuum method for modelling surface tension" *J. Comput. Phys.* **100**(2) 335-354
- Bernardi, D., M., M. W. Verbrugge, (1992). "A Mathematical Model of the Solid Polymer Electrolyte Fuel Cell", *J. Electrochem. Soc.* **139**(9): 2477-2491.
- Bernardi, D. M. (1990). "Water-Balance Calculations for Solid-Polymer-Electrolyte Fuel Cells" *J. Electrochem. Soc.* **137**(11): 3344-3350
- Beyers, D., M. Wo"hr, et al. (1997). "Simulation of a polymer electrolyte fuel cell electrode." *Journal of Applied Electrochemistry* **27**(11): 1254-1264
- Biyikoğlu A. (2005). "Review of proton exchange membrane fuel cell models" *International Journal of Hydrogen Energy* **30**(11): 1181-1212
- Bird, R. B., W. E. Stewart, E. N. Lightfoot, (1960). "Transport phenomena", John Wiley & Sons
- Carcadea, E., H. Ene, et al. (2005). "Numerical simulation of mass and charge transfer for a PEM fuel cell." *International Communications in Heat and Mass Transfer* **32**(10): 1273-1280.
- Chan, S. H., S. K. Goh and S. P. Jiang, (2003). "A mathematical model of polymer electrolyte fuel cell with anode CO kinetics" *Electrochimica Acta* **48**(13): 1905-1919
- Dannenberg, K., P. Ekdunge, et al. (2000). "Mathematical model of the PEMFC." *Journal of Applied Electrochemistry* **30**(12): 1377-1387.
- Dawes, J. (2007) "An Investigation into the Effects of Flooding in PEM Fuel Cells, Part 1: Flooding Model", MSc Thesis: University of Manchester.
- Dawes, J, Hanspal, N.S., Turan, A. (2008) "Percolation Theory and Network Models applied to Flooding in PEM Fuel Cells", *ASME Journal of Fuel Cells* (*under review*).
- Dutta, S., S. Shimpalee, J. W. Van Zee, (2001). "Numerical prediction of mass-exchange between cathode and anode channels in a PEM fuel cell" *International Journal of Heat and Mass Transfer* **44**(11): 2029-2042
- Eaton B, et al (2001). "One-dimensional, transient model of heat, mass, and charge transfer in a proton exchange membrane" *Advanced Energy Systems Division (Publication) AES*, American Society of Mechanical Engineers; **41**: 429-440.
- Eikerling, M. and A. A. Kornyshev (1998). "Modelling the performance of the cathode catalyst layer of polymer electrolyte fuel cells." *Journal of Electroanalytical Chemistry* **453**(1-2): 89-106.

- Fontes & Nilsson (2001), *Industrial Physicist*, tipmagazine.com
- Fuller, T., F. and J. Newman (1993). "Water and Thermal Management in Solid Polymer Electrolyte Fuel Cells" *J. Electrochem. Soc.* **140**(5): 1218-1225
- Gallart, M.S. (2004) "Computational Modeling and Optimization of Proton Exchange Membrane Fuel Cells" PhD thesis, University of Victoria.
- Gurau V., H. T. Liu, S. Kakac (1998). "Two-dimensional model for proton exchange membrane fuel cells" *AIChE J* **44**(11): 2410 - 2422
- Garboczi, E., D. Bentz, (1992). "Computer simulation of the diffusivity of cement-based materials" *Journal of Material Science* **27**: 2083 - 2092
- Hirschenhofer, J. H., D. B. Stauffer, et al. (1994). *Fuel cells: A handbook (Revision 3)*
- Hontanon, E., M. J. Escudero, et al. (2000). "Optimisation of flow-field in polymer electrolyte membrane fuel cells using computational fluid dynamics techniques." *Journal of Power Sources* **86**(1-2): 363-368.
- Hsing, I. M. and P. Futerko (2000). "Two-dimensional simulation of water transport in polymer electrolyte fuel cells." *Chemical Engineering Science* **55**(19): 4209-4218.
- Huang Z., (2000). "Experimental and Mathematical Studies of PEM Fuel Cell Performances" University of Miami, M.S.Thesis.
- Janssen G.J.M. (2001). "A phenomenological model of water transport in a proton exchange membrane fuel cell" *J. Electrochem. Soc.* **148** (12): A1313–A1323
- Jiao K, B. Zhou, P. Quan (2006). "Liquid water transport in straight micro-parallel-channels with manifolds for PEM fuel cell cathode" *Journal of Power Sources* **157**(1): 226-243
- Kaviany, M. (1991). "Principles of Heat Transfer in Porous Media", Springer, NY
- Larminie, J., A. Dicks (2003) "Fuel Cell Systems Explained" 2nd Edition, John Wiley & Sons
- Lum K., W. and J. J McGuirk, (2005) "Three-dimensional model of a complete polymer electrolyte membrane fuel cell - model formulation, validation and parametric studies", *Journal of Power Sources* **143**(1-2): 103-124.
- Maggio, G., V. Recupero, et al. (2001). "Modeling polymer electrolyte fuel cells: an innovative approach." *Journal of Power Sources* **101**(2): 275-286.
- Maxoulis, C. N., D. N. Tsinoglou, et al. (2004). "Modeling of automotive fuel cell operation in driving cycles." *Energy Conversion and Management* **45**(4): 559-573.
- Mazumder, S; Cole, J V, (2003). 'Rigorous 3-D Mathematical Modeling of PEM Fuel Cells: I. Model Predictions without Liquid Water Transport', *Journal of the Electrochemical Society.* **150**(11): A1503-A1509.
- Mazumder, S; Cole, J V, (2003). 'Rigorous 3-D Mathematical Modeling of PEM Fuel Cells: II. Model Predictions with Liquid Water Transport.', *Journal of the Electrochemical Society.* **150**(11): A1510-A1517.
- McNaught A. D., A. Wilkinson, (1997). 'IUPAC Compendium of Chemical Terminology 2nd Edition'

- Nam, J., M. Kaviany (2003). 'Effective diffusivity and water-saturation distribution in single and two layer PEMFC diffusion medium' *International Journal of Heat and Mass Transfer* **46**(24): 4595-4611
- Nguyen T. V., White R. E. (1993) "A water and heat management models for proton-exchange-membrane fuel cells" *J. Electrochem. Soc.* **140**: 2178–2186
- Nguyen PT, Berning T, Djilali N. (2004) "Computational model of a PEMFC with serpentine gas flow channels" *J. Power Sources* **130**: 149–157
- Natarajan, D. and T. Van Nguyen (2003). "Three-dimensional effects of liquid water flooding in the cathode of a PEM fuel cell." *Journal of Power Sources* **115**(1): 66-80
- Pharoah, J. G., K. Karan, et al. (2006). "On effective transport coefficients in PEM fuel cell electrodes: Anisotropy of the porous transport layers." *Journal of Power Sources* **161**(1): 214-224
- Rowe, A. and X. Li (2001). "Mathematical modeling of proton exchange membrane fuel cells." *Journal of Power Sources* **102**(1-2): 82-96
- Sahimi, M. (1994). "Applications of Percolation theory" Taylor and Francis (CRC Press), ISBN: 9780748400768
- Scott, K. *et al.* (2000), Modeling transport phenomena and performance of Direct Methanol Fuel Cell Stacks, *Chem. Engg. Res & Des*, **78**: 881-888
- Selyakov, V. I. and V. V. Kadet (1996). 'Percolation Models for transport in Porous Media: With Applications to Reservoir Engineering' Springer, Theory and Applications of Transport in Porous Media Vol. 9. ISBN: 978-0-7923-4322-6
- Siegel, N. P., M. W. Ellis, et al. (2004). "A two-dimensional computational model of a PEMFC with liquid water transport." *Journal of Power Sources* **128**(2): 173-184
- Sivertsen B.R. and N. Djilali (2005) "CFD-based modelling of proton exchange membrane fuel cells" *Journal of Power Sources* **141**(1): 65-78
- Slattery, J.C., Bird, R.B., (1958). "Calculation of the diffusion coefficient of dilute gases and of the self-diffusion coefficient of dense gases" *AIChE J* **4**(2): 137-142
- Sousa, J. R. and E. R. Gonzalez (2005). "Mathematical modeling of polymer electrolyte fuel cells." *Journal of Power Sources* **147**(1-2): 32-45
- Springer, T. E., T. A. Zawodzinski, S. Gottesfeld (1991) "Polymer Electrolyte Fuel Cell Model" *Journal Electrochem. Soc.* **138**(8): 2334-2342
- Squadrito, G., G. Maggio, et al. (1999). "An empirical equation for polymer electrolyte fuel cell (PEFC) behaviour." *Journal of Applied Electrochemistry* **29**(12): 1449-1455
- Standaert, F., K. Hemmes, et al. (1996). "Analytical fuel cell modeling." *Journal of Power Sources* **63**(2): 221-234
- Standaert, F., K. Hemmes, et al. (1998). "Analytical fuel cell modeling; non-isothermal fuel cells." *Journal of Power Sources* **70**(2): 181-199

- Tomadakis M., M., S. V. Sotirchos (1993). "Ordinary and transition regime diffusion in random fibre structures" *AICHE J.* 39: 397-412
- Tseng C., S. Lou, Y. Yan, L. Sung (2005). "Gas Diffusion Layer and Microporous Layer for PEMFC" Proceedings International Hydrogen Energy Conference and Exhibition IHEC 2005 Istanbul, Turkey
- Tafel, J., K. Schmitz, K. Naremann, B. Emmert, (1905). "Concerning the polarisation during cathodic evolution of hydrogen" *Z Phys. Chem.*, 50A:641
- Um S, Wang CY, Chen KS. (2000) "Computational fluid mechanics of proton exchange membrane fuel cells." *J Electrochem Soc* **147**:4485–4493
- Um S., C. Y. Wang (2004). "Three-dimensional analysis of transport and electrochemical reactions in polymer electrolyte fuel cells" *J Power Sources* **125**(1): 40–51
- Wang C. Y., P. Cheng (1997). "A multiphase mixture model for multiphase, multi-component transport in capillary porous media. I. Model development" *Int. J. Heat Mass Transfer* **39**(17): 3607-3618
- Wang J.T., R.F. Savinell, J.S. Wainright, M. Litt and H. Yu, (1996). "A H₂/O₂ fuel cell using acid doped polybenzimidazole as polymer electrolyte" *Electrochim Acta* **41**: 193–197
- Wang ZH, Wang CY, Chen KS (2001). "Two-phase flow and transport in the air cathode of proton exchange membrane fuel cells." *J Power Sources* (94): 40–50
- Weast R.C., M.J. Astle (Eds.), *CRC Handbook of Chemistry and Physics*, 62nd ed., CRC Press, Florida, 1981.
- Wöhr M., K. Bolwin, W. Schnurnberger, M. Fischer, W. Neubrand and G. Eigenberger (1998) "Dynamic modelling and simulation of a polymer membrane fuel cell including mass transport limitation" *International Journal of Hydrogen Energy* **23**(3): 213-218
- Yi, sJ. S., J. D. Yang, C. King, (2004). "Water management along the flow channels of PEM fuel cells" *AICHE Journal* **50**(10): 2594 - 2603
- Yi J. S., T. V. Nguyen (1998) "An along the channel model for proton exchange membrane fuel cells" *J Electrochem Soc* **145**(4): 1149–1159.
- You, L; Liu, H. (2006) 'A two-phase flow and transport model for PEM fuel cells', *Journal of Power Sources* **155**(2) 219-230
- Ying W., Y-J. Sohn, W-Y. Lee, J. Ke, C-S. Kim (2005) "Three-dimensional modeling and experimental investigation for an air-breathing polymer electrolyte membrane fuel cell (PEMFC)" *Journal of Power Sources* **145**(2): 563-571
- Van Bussel, H. P. L. H., F. G. H. Koene, et al. (1998). "Dynamic model of solid polymer fuel cell water management." *Journal of Power Sources* **71**(1-2): 218-222.

Figure Captions

- Figure 1. Numerical algorithm.
- Figure 2. Geometry and computational domain.
- Figure 3. Width averaged current density at very high humidity conditions GDL permeability = $5 \times 10^{-11} \text{m}^2$ – Validation against Shimpalee *et al.* (2000).
- Figure 4: Velocity vectors shown at streamwise slices at very high humidity in the gas channels, GDL permeability = $5 \times 10^{-11} \text{m}^2$, fully developed velocity profiles are shown enlarged.
- Figure 5: Velocity vectors shown at streamwise slices at very high humidity in the porous zones GDL permeability = $5 \times 10^{-11} \text{m}^2$.
- Figure 6a. 3D Gauge pressure contours for very high humidity, GDL permeability = $5 \times 10^{-11} \text{m}^2$ case.
- Figure 6b. Gauge pressure contours for very high humidity, GDL permeability = $5 \times 10^{-11} \text{m}^2$ case at $Z = 0.05$ slice.
- Figures 7a,b,c. Velocity vectors at midway slice for high humidity GDL permeability = $5 \times 10^{-10} \text{m}^2$ (a), $5 \times 10^{-11} \text{m}^2$ (b) and $5 \times 10^{-12} \text{m}^2$ (c) case, arrow direction and colour show direction and magnitude.
- Figures 8. Width averaged pressure drops at across the anode and cathode GDLs at the inlet, midway along the channel and the outlet for high humidity GDL permeability = $5 \times 10^{-10} \text{m}^2$ (a), $5 \times 10^{-11} \text{m}^2$ (b) and $5 \times 10^{-12} \text{m}^2$ (c) case.
- Figure 9: Oxygen volume fraction contour plot shown at longitudinal slices for high humidity GDL permeability = $5 \times 10^{-11} \text{m}^2$ case.
- Figure 10: Water vapour volume fraction contour plot with relative humidity = 100% iso-surface for high humidity GDL permeability = $5 \times 10^{-11} \text{m}^2$ case.
- Figure 11: Effect of GDL permeability on width averaged current density shown for very high humidity GDL permeability = $5 \times 10^{-11} \text{m}^2$ case.
- Figure 12: Effect of gas diffusivity coefficients on width averaged current density shown for very high humidity GDL permeability = $5 \times 10^{-11} \text{m}^2$ case.
- Figure 13: Comparison of diffusivity models, width averaged current density shown at very high humidity, GDL permeability = $5 \times 10^{-11} \text{m}^2$.
- Figure 14: Global validation with variable inlet humidity, comparison against the numerical model and experiment data from Lum *et al.* (2005).

Table Captions

Table 1: Governing Equations

Table 2: Auxiliary Equations

Table 3 a&b: Physical Parameters

Table 4: Numerical Parameters

Table 5: Parametric study parameters **TABLE 1**

Description	Equation	
Momentum equation	$\nabla \cdot (\rho \vec{u}\vec{u}) = -\nabla P + \nabla \cdot (\mu \nabla \vec{u}) + S_u$	(1)
Darcy momentum term	$\nabla P = -\frac{\mu \vec{u}}{k_i}$	(2)
Continuity equation	$\nabla \cdot (\rho \vec{u}) = S_m$	(3)
Source term at anode CL	$S_m = S_{O_2} + S_{cw}$	(4)
Source term at cathode CL	$S_m = S_{H_2} + S_{aw}$	(5)
Species transport equations	$\nabla \cdot (\rho \vec{u} \vec{X}_k) = \nabla \cdot (D_k^{eff} \rho \nabla \vec{X}_k) + S_k$	(6)
Consumption of hydrogen due to electrochemical effects at the anode	$S_{H_2} = -\frac{I(x,y)}{2F} M_{H_2} A_{cv}$	(7)
Consumption of oxygen due to electrochemical effects at the cathode	$S_{O_2} = -\frac{I(x,y)}{4F} M_{O_2} A_{cv}$	(8)
Production of water and flux of water due to electrochemical effects at the cathode	$S_{cww} = \frac{1+2\alpha(x,y)}{2F} I(x,y) M_{H_2O} A_{cv}$	(9)
Flux of water due to electrochemical effects at the anode	$S_{awv} = -\frac{\alpha(x,y)}{F} I(x,y) M_{H_2O} A_{cv}$	(10)

TABLE 2

Description	Equation	
Binary diffusion coefficients	$P \cdot D_{AB} = a \left(\frac{T}{\sqrt{T_{cA} T_{cB}}} \right)^b (P_{cA} P_{cB})^{1/3} (T_{cA} T_{cB})^{5/12} \left(\frac{1}{M_A} + \frac{1}{M_B} \right)^{1/2} \epsilon^{1.5}$	(11)
Net water transport coefficient	$\alpha(x, y) = n_d(x, y) - \frac{FD_w(x, y) \{c_{w,c}(x, y) - c_{w,a}(x, y)\}}{I(x, y)t_m}$	(12)
Local current density	$I(x, y) = \frac{\sigma_m(x, y)}{t_m} [V_{oc} - V_{cell} - \eta(x, y)]$	(13)
Reaction overpotential	$\eta(x, y) = \frac{RT}{0.5F} \ln \left[\frac{1.013 \times 10^5 \times I(x, y)}{I_{0C} P_{O_2}(x, y)} \right] + \frac{RT}{F} \ln \left[\frac{1.013 \times 10^5 \times I(x, y)}{I_{0A} P_{H_2}(x, y)} \right]$	(14)
Membrane conductivity	$\sigma_m(x, y) = 100 \left[0.00514 \left(\frac{M_{m,dry}}{\rho_{m,dry}} \right) c_{w,a}(x, y) - 0.00326 \right] \times \exp \left[1268 \left(\frac{1}{303} - \frac{1}{T} \right) \right]$	(15)
Water concentration	$c_{w,k}(x, y) = \frac{\rho_{m,dry}}{M_{m,dry}} (0.043 + 17.8a_k - 39.8a_k^2 + 36.0a_k^3)$ if $a_k \leq 1$	(16)
	$c_{w,k}(x, y) = \frac{\rho_{m,dry}}{M_{m,dry}} (14 + 1.4(a_k - 1))$ if $a_k > 1$	(17)
Water activity	$a_k(x, y) = \frac{X_{w,k}(x, y)P(x, y)}{P_{w,k}^{sat}}$	(18)
Water vapour saturation pressure	$P_{w,k}^{sat} = [0.00644367 + 0.000213948(T - 273.0) + 3.43293 \times 10^{-5}(T - 273.0)^2 - 2.70381 \times 10^{-7}(T - 273.0)^3 + 8.77696 \times 10^{-9}(T - 273.0)^4 - 3.14035 \times 10^{-13}(T - 273.0)^5 + 3.82148 \times 10^{-14}(T - 273.0)^6] \times 1.013 \times 10^5$	(19)
Electro-osmotic drag coefficient	$n_d(x, y) = 0.0049 + 2.02a_a - 4.53a_a^2 + 4.09a_a^3$ if $a_a \leq 1$ $n_d(x, y) = 1.59 + 0.159(a_a - 1)$ if $a_a > 1$	(20)
Water diffusion coefficient	$D_w = n_d \times 5.5 \times 10^{-11} \exp \left[2416 \left(\frac{1}{303} - \frac{1}{T} \right) \right]$	(21)

TABLE 3 A,B

Description	Low Humidity	High Humidity	Very High Humidity	Units
Anode inlet velocity	1.83	2.21	2.56	ms ⁻¹
Anode inlet mass fraction of hydrogen	0.635	0.406	2.595	-
Anode inlet mass fraction of water vapour	0.365	0.594	0.705	-
Cathode inlet velocity	7.91	9.05	12.9	ms ⁻¹
Cathode inlet mass fraction of oxygen	0.225	0.21	0.187	-
Cathode inlet mass fraction of nitrogen	0.734	0.705	0.61	-
Cathode inlet mass fraction of water vapour	0.041	0.085	0.203	-

Symbol	Description	Value	
P_0	Operating pressure	101325 Pa	
T_0	Operating temperature	345 K	
k_i	GDL Permeability	$5 \times 10^{-11} \text{ m}^2$	
F	Faradays constant	96485.3 C mol ⁻¹	
-	-	Water	Other species
a	Binary diffusivity equation coefficients	3.64×10^{-4}	2.745×10^{-4}
b		2.334	1.832
ε	GDL porosity	0.65	
t_m	Membrane thickness	0.1270 mm	
V_{oc}	Open circuit voltage	1.1 V	
V_{cell}	Cell voltage	0.53 V	
I_{0A}	Exchange current densities	100 A m ⁻²	
I_{0C}		1000 A m ⁻²	
R	Gas constant	$8.3144 \text{ mol}^{-1} \text{ K}^{-1}$	
$M_{m,dry}$	Dry mass of membrane	1.1 kg mol ⁻¹	
$\rho_{m,dry}$	Dry density of membrane	2000 kg m ⁻³	
v	Correlation index	0.90	
P_c	Percolation threshold	0.11	

TABLE 4

Description	Value
Number of cells	14114
Number of iterations	~250
Convergence criteria	10^{-6}
Numerical scheme	Second order upwinding
Computational time	~ 30 mins
Anode inlet mass flux	$-3.9 \times 10^{-13} \text{ kg/m}^3\text{s}$
Anode outlet mass flux	$-9.4 \times 10^{-12} \text{ kg/m}^3\text{s}$
Cathode inlet mass flux	$3.16 \times 10^{-13} \text{ kg/m}^3\text{s}$
Cathode outlet mass flux	$9.53 \times 10^{-12} \text{ kg/m}^3\text{s}$
Total	$-2.27 \times 10^{-19} \text{ kg/m}^3\text{s}$

TABLE 5

Parameter	Value
DSF1	140%
DSF2	120%
DSF3	100%
DSF4	80%
DSF5	60%
DSF6	40%
k1	$1.5 \times 10^{-8} \text{ m}^2$
k2	$1.5 \times 10^{-9} \text{ m}^2$
k3	$1.5 \times 10^{-10} \text{ m}^2$
k4	$1.5 \times 10^{-11} \text{ m}^2$
k5	$1.5 \times 10^{-12} \text{ m}^2$

FIG:1

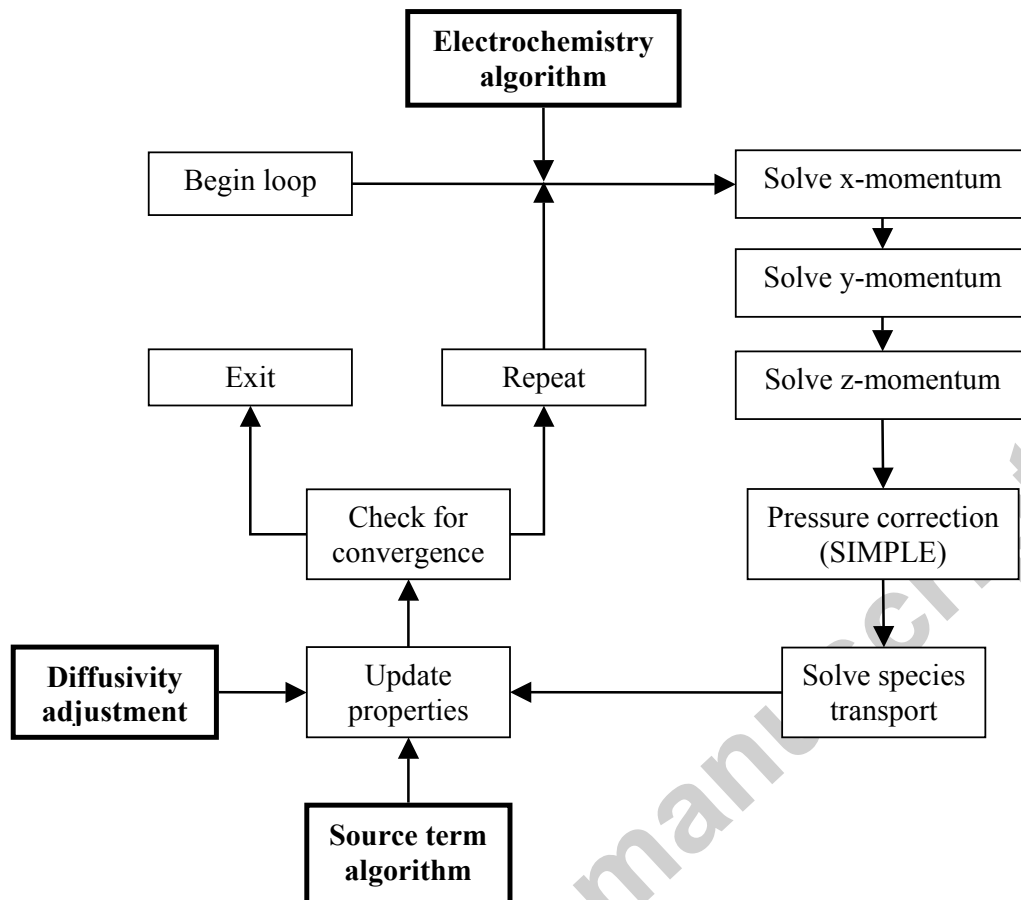


FIG:2

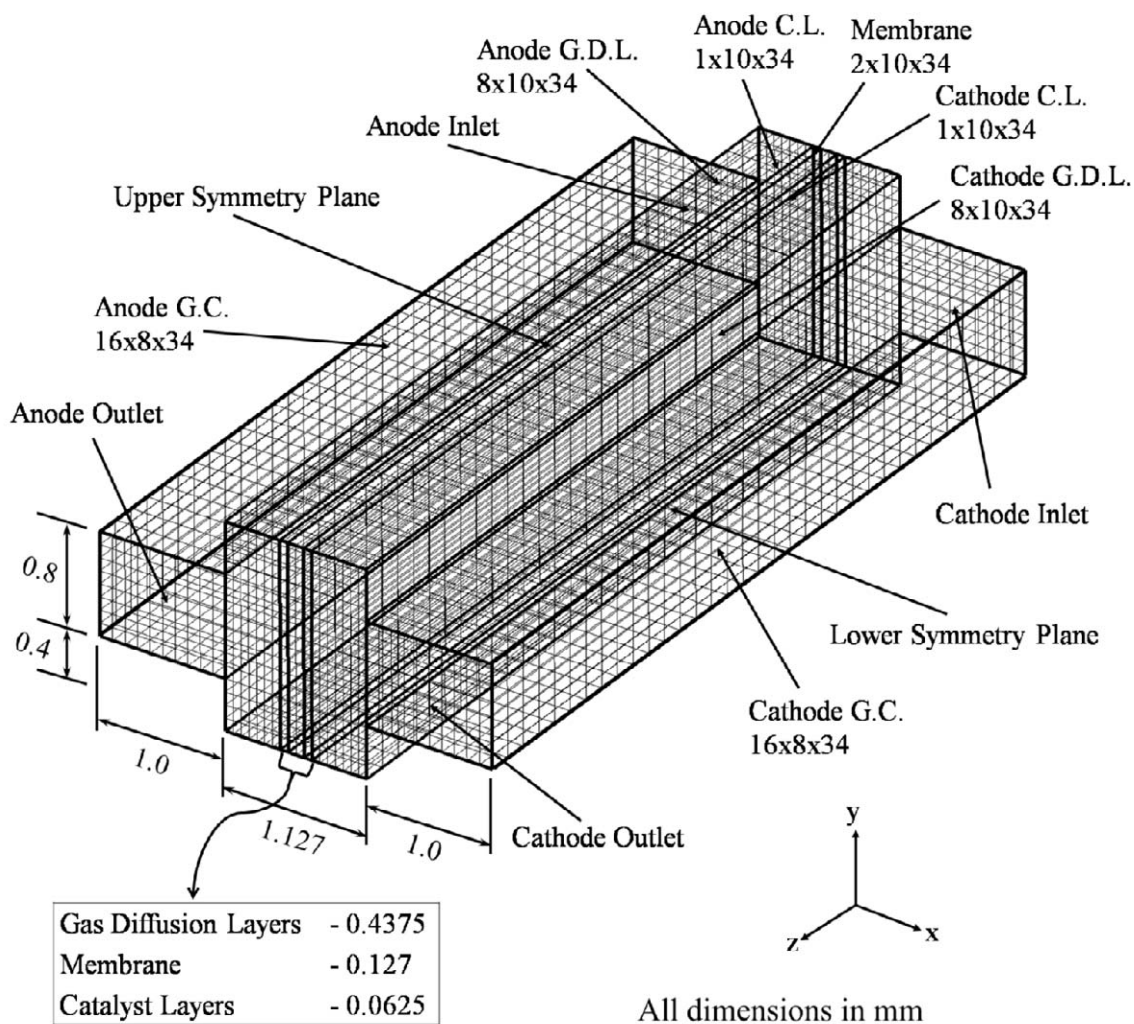


FIG:3

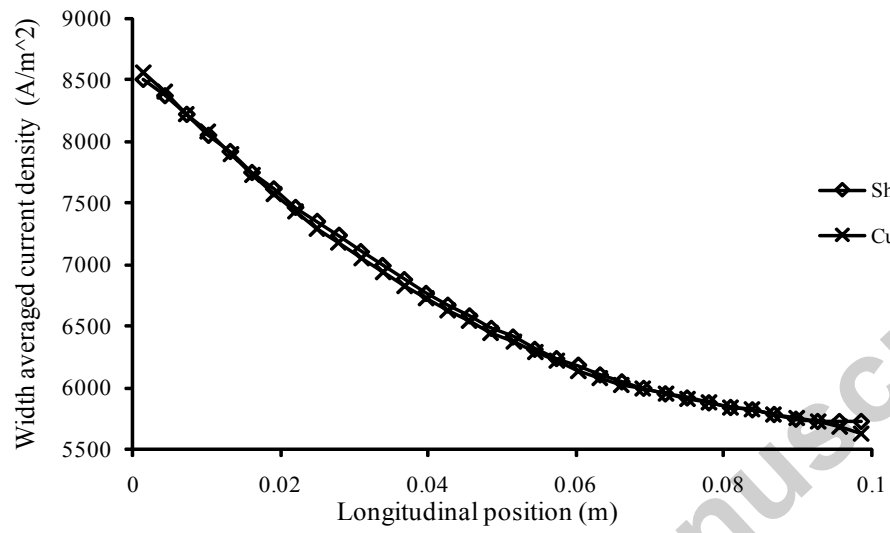
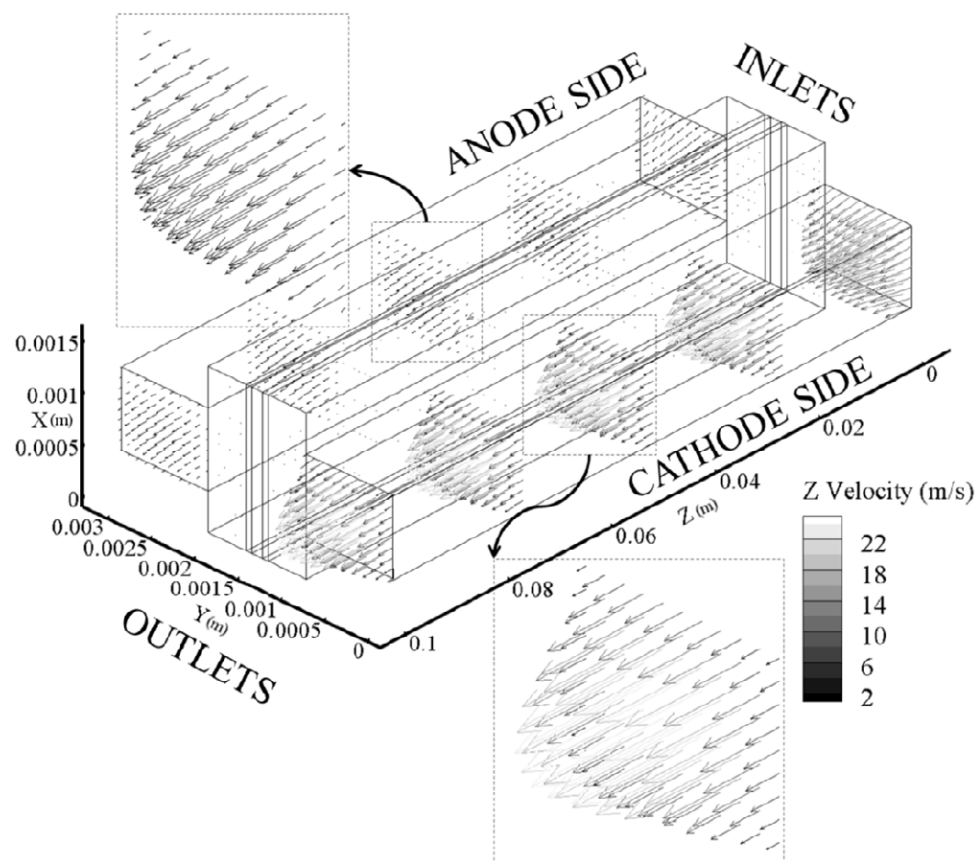
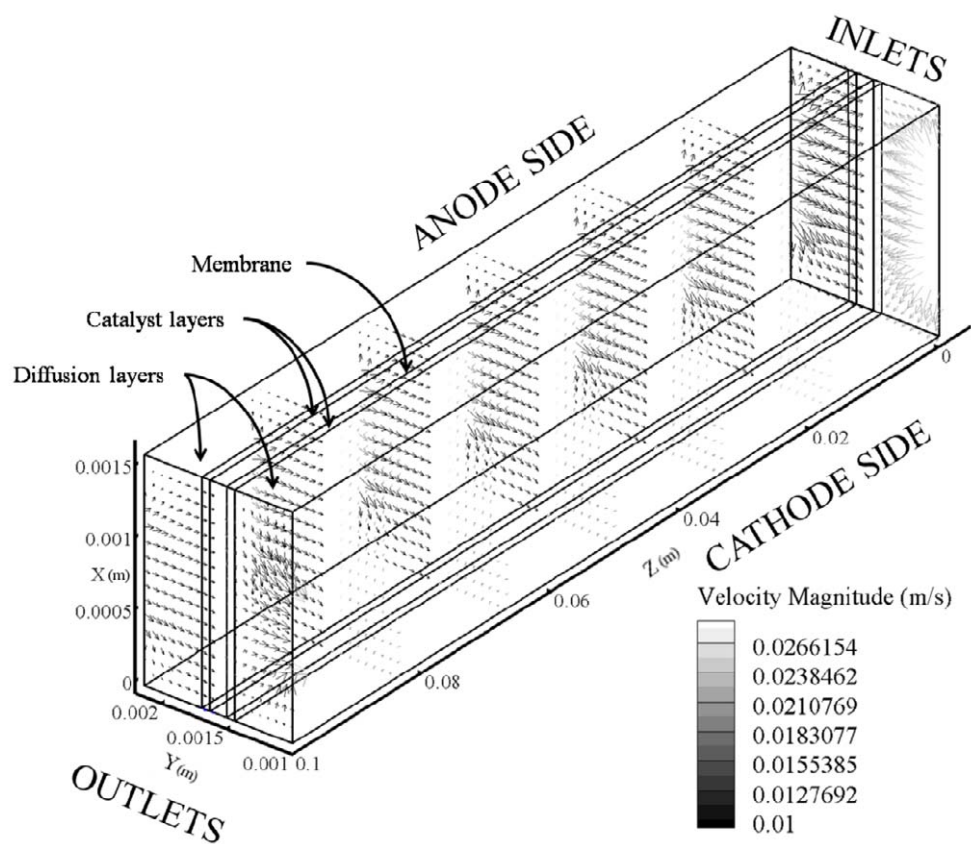


FIG:4



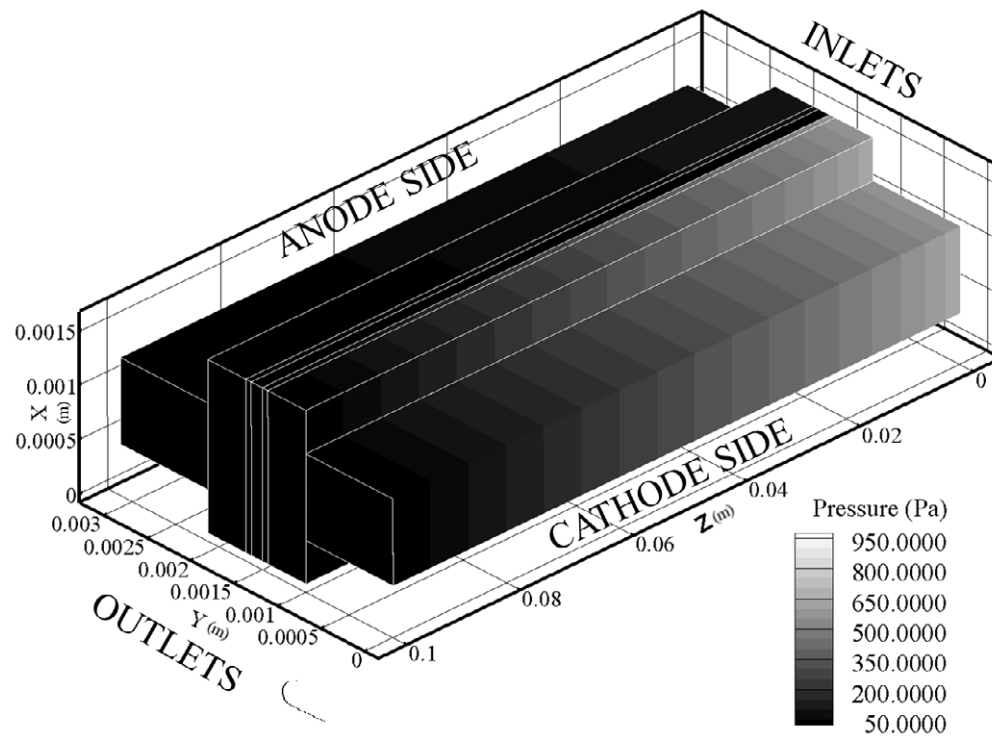
ACCEPTED

FIG:5



Accepted

FIG:6



Accepted m

FIG:7(a)

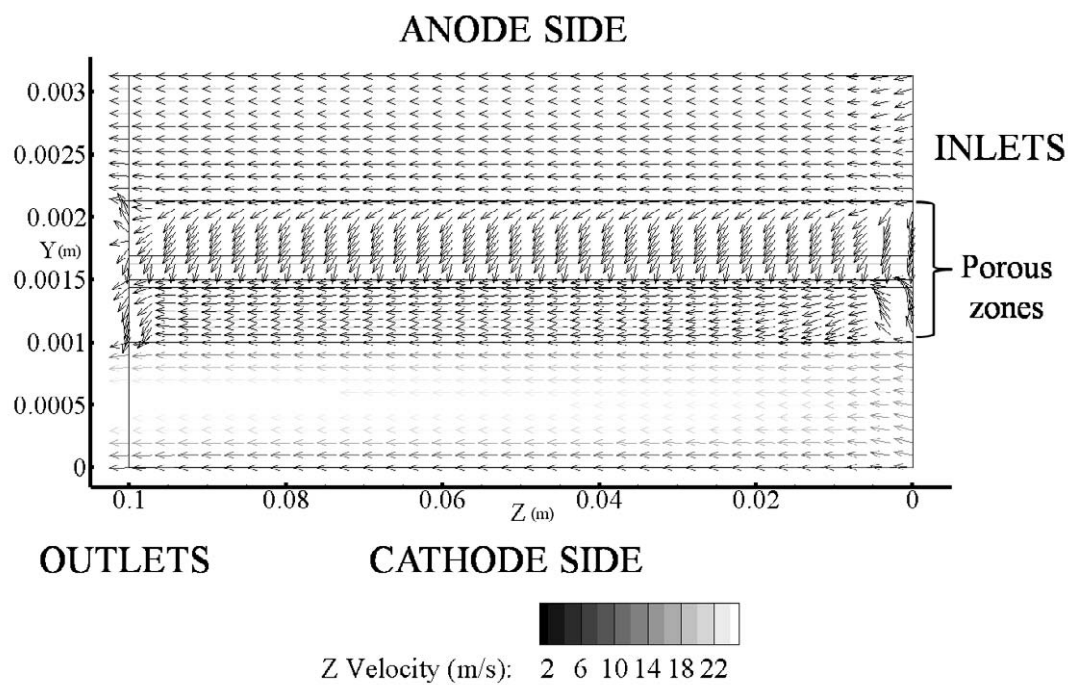
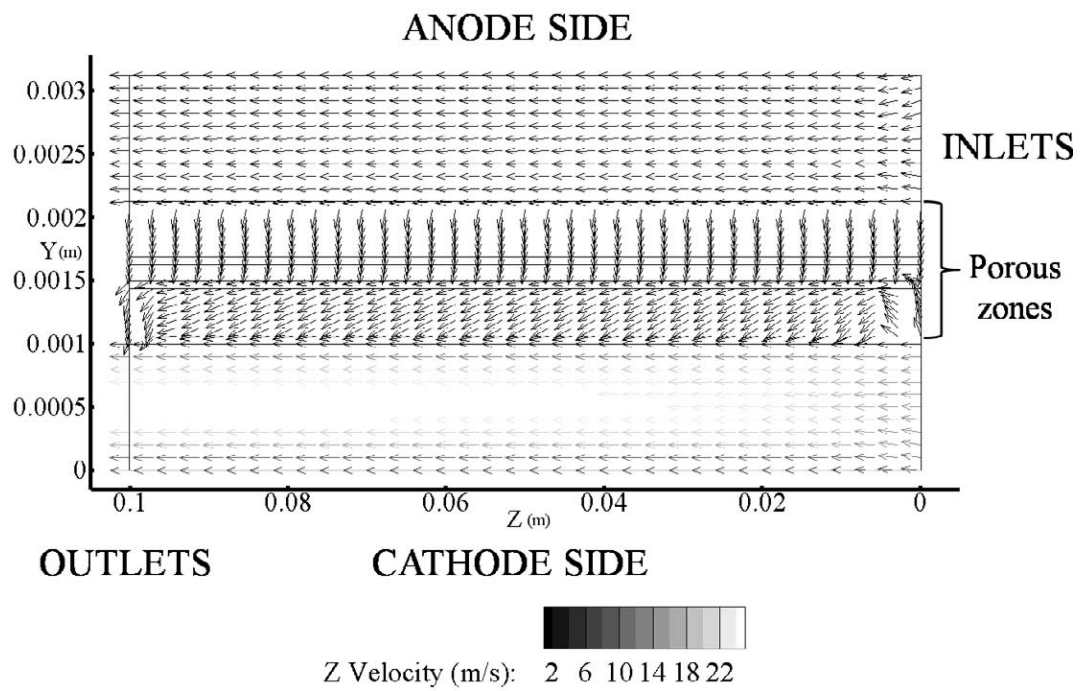


FIG:7(b)



Accepted m

FIG:7©

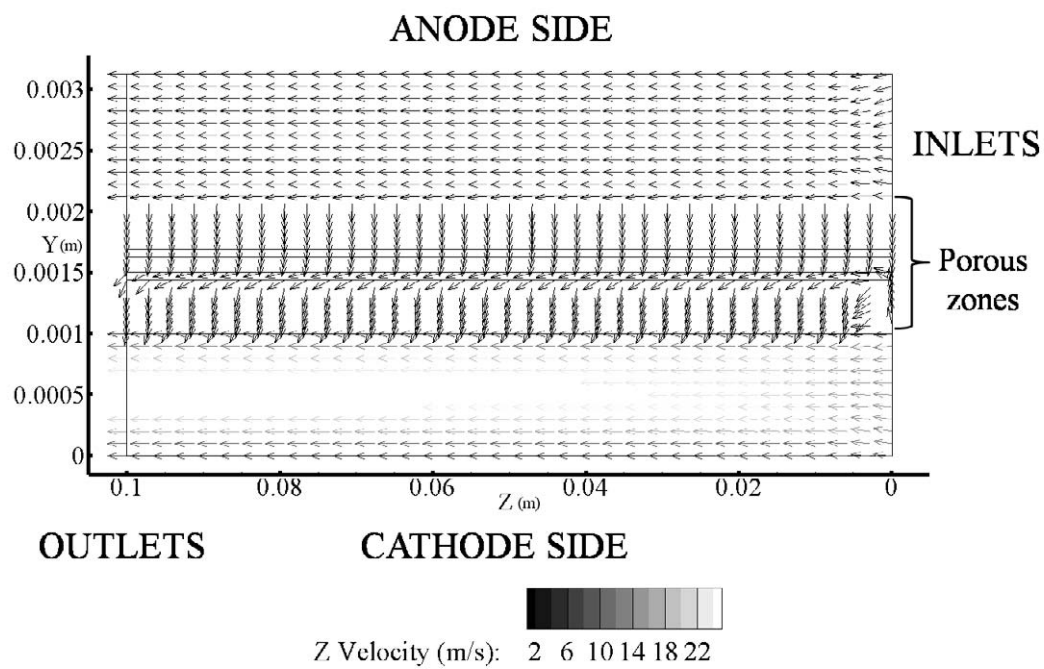
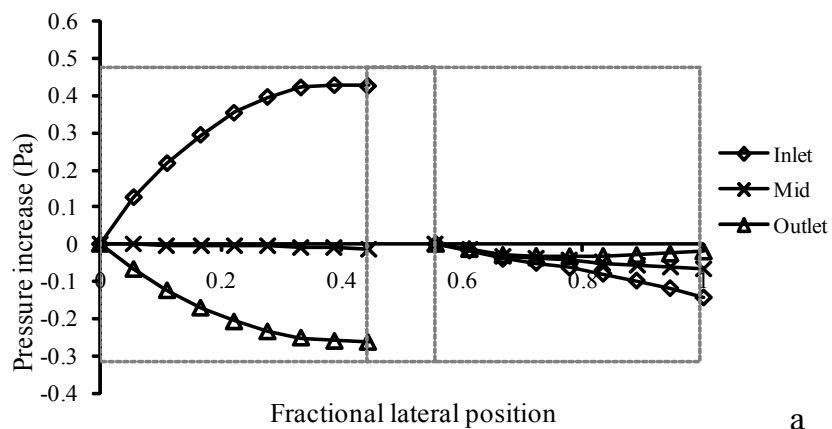
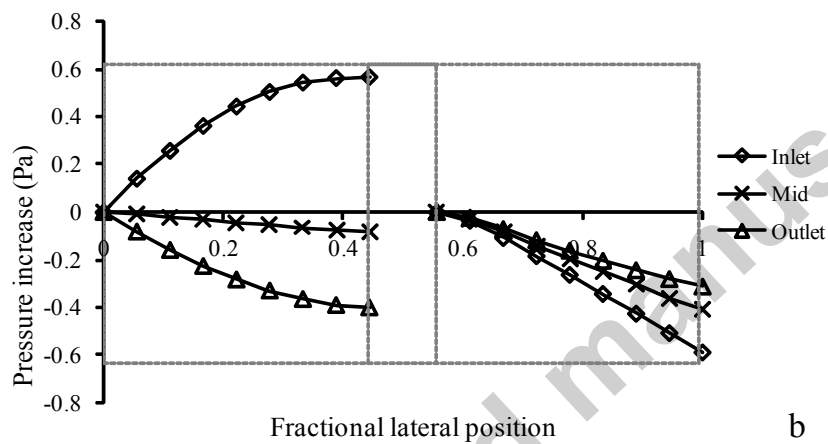


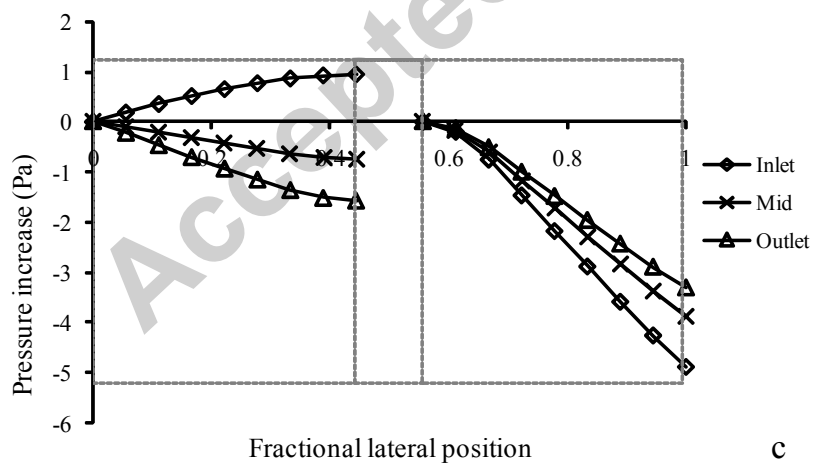
FIG:8(A, B, C)



a



b



c

FIG:9

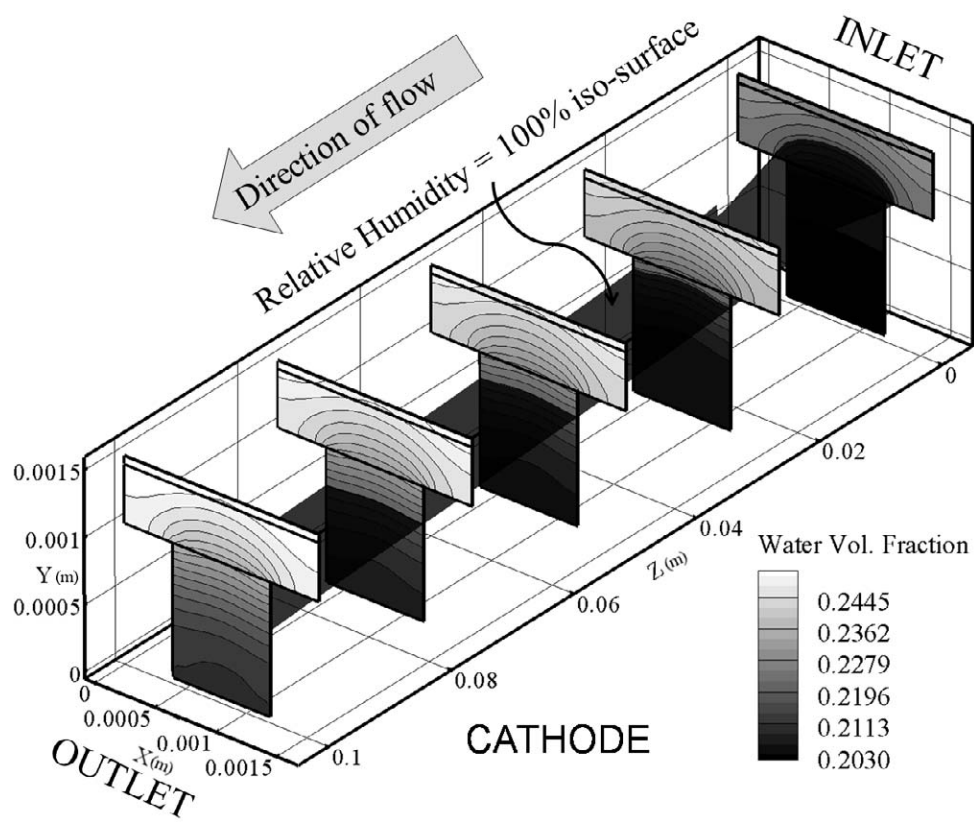
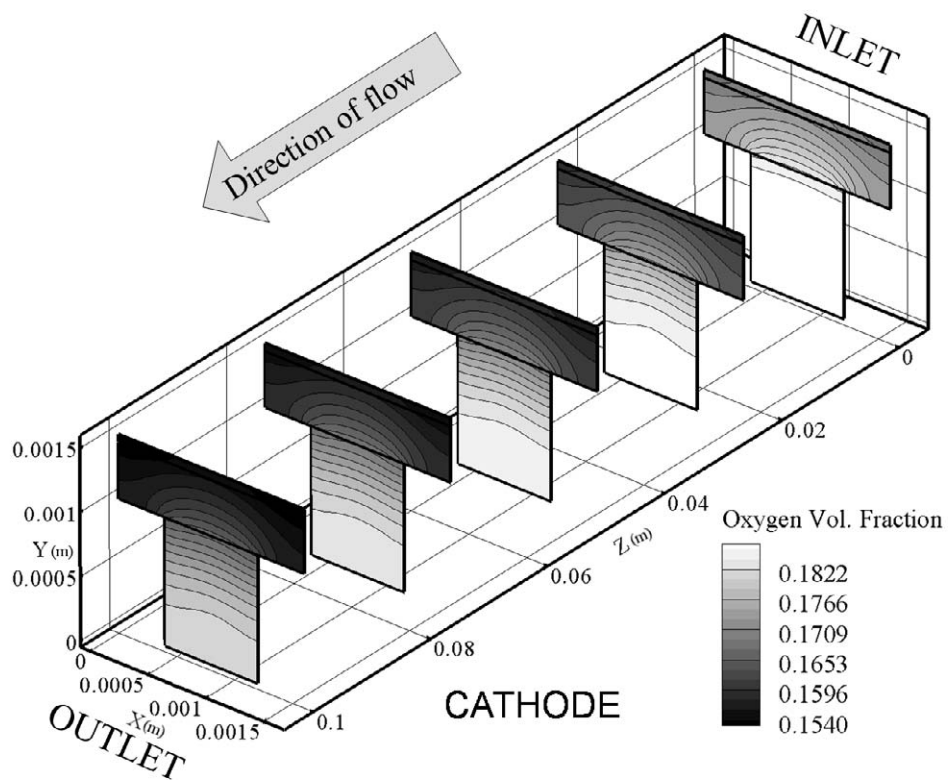


FIG:10



Accepted m

FIG 11

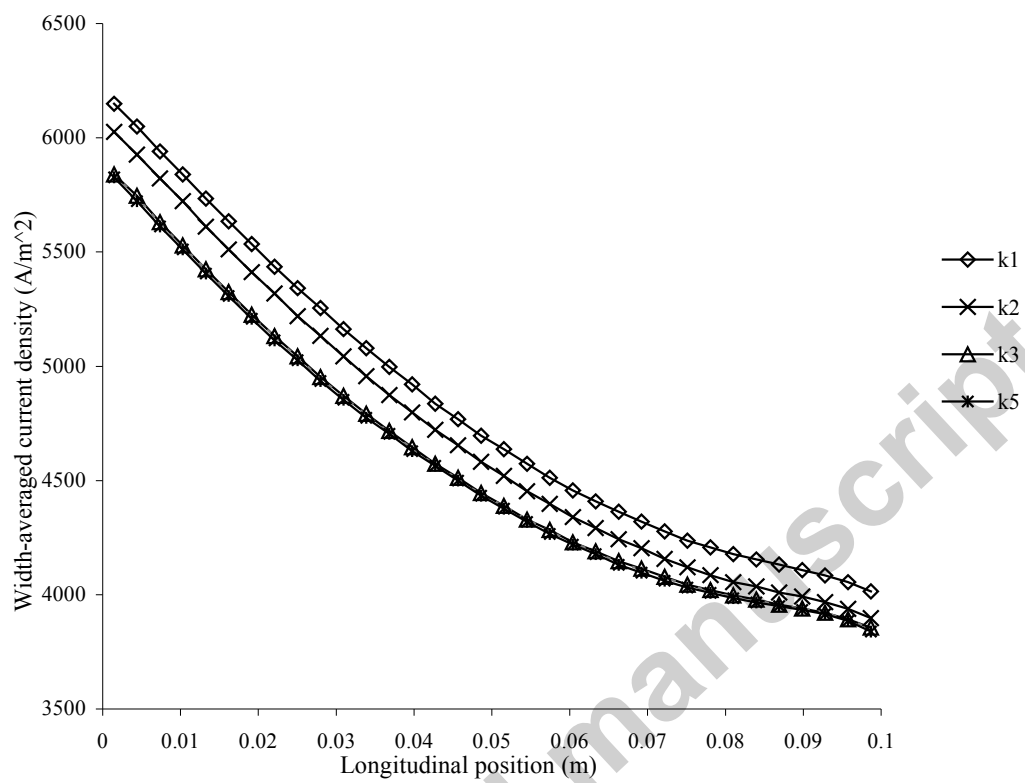


FIGURE 12

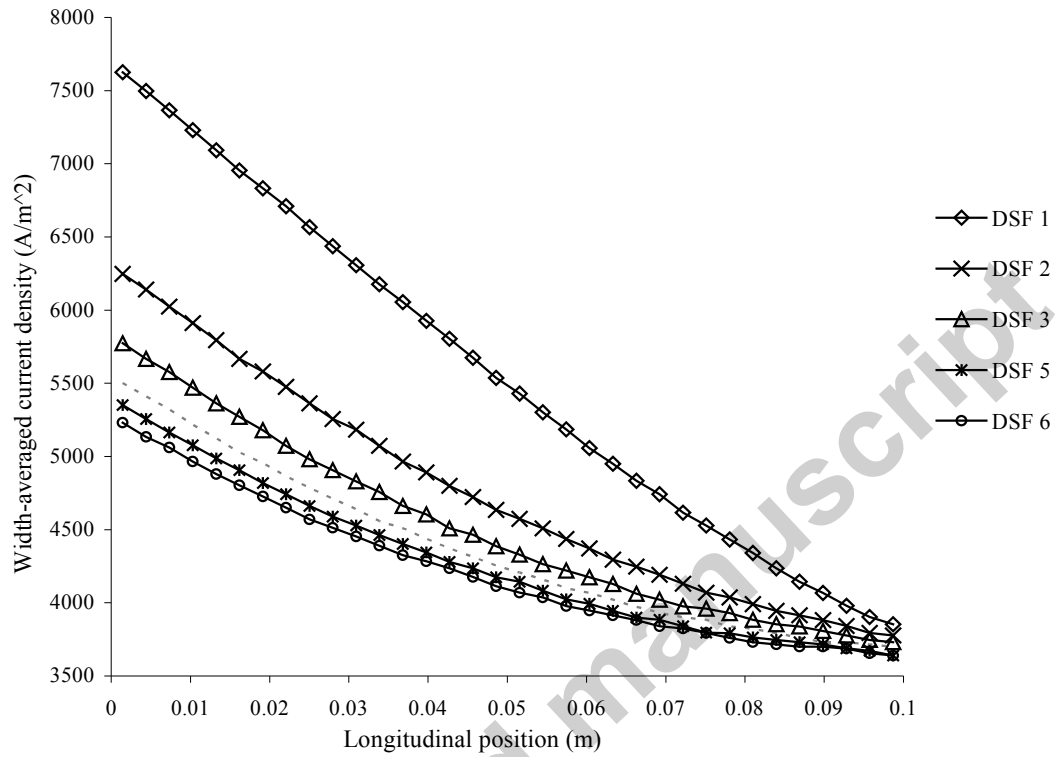


FIGURE 13

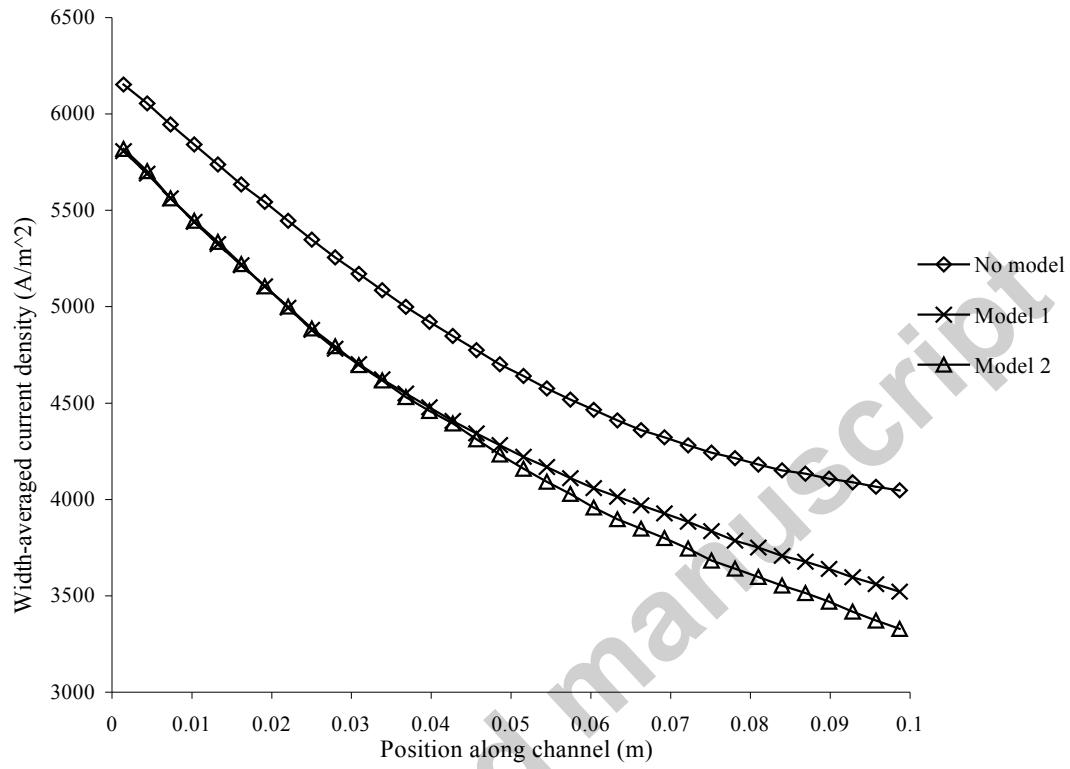


FIGURE 14

